Marine and Petroleum Geology 127 (2021) 104955

Contents lists available at ScienceDirect

Marine and Petroleum Geology

journal homepage: www.elsevier.com/locate/marpetgeo

Research paper

Source rock potential, crude oil characteristics and oil-to-source rock correlation in a Central Paratethys sub-basin, the Hungarian Palaeogene Basin (Pannonian basin)

Sándor Körmös [a,b,*], Reinhard F. Sachsenhofer [b], Achim Bechtel [b], Balázs Géza Radovics [c], Katalin Milota [c], Félix Schubert [a]

[a] University of Szeged, Department of Mineralogy, Geochemistry and Petrology, Egyetem u. 2, H-6722, Szeged, Hungary
[b] Montanuniversität Leoben, Chair in Petroleum Geology, Peter-Tunner-str. 5, A-8700, Leoben, Austria
[c] MOL Plc., Október huszonharmadika u. 18, H-1117, Budapest, Hungary

ARTICLE INFO

Keywords:
Central Paratethys
Hungarian Palaeogene Basin
Crude oil
Source rocks
Oil-to-source rock correlation
Compound-specific isotope

ABSTRACT

Eocene and Lower Oligocene rocks are potential source rocks for crude oil accumulations in the Hungarian Palaeogene Basin. To enhance the understanding of the hydrocarbon system, this study (i) assesses the petroleum potential of Palaeogene formations, (ii) characterises the source rock facies of the accumulated oils, and (iii) provides an oil-to-source correlation. Rock-Eval data of samples from three boreholes (W–1, W–9 and W–12) show that most Palaeogene formations are mature at depths exceeding 2.1–2.5 km. The coal-bearing Kosd Formation includes good to excellent gas- (and oil-) prone source rocks. The overlying Buda Marl Formation is typically organic matter-lean but contains oil-prone rocks with up to 2.3 wt% TOC and a fair petroleum potential in borehole W–9. The Tard Clay Formation in W–12 reaches up to 1.9 wt% TOC and shows HI values up to 440 mg HC/g TOC, characterising the deposits as good petroleum source rocks. Based on low TOC contents, the Kiscell Clay Formation is not considered a source rock. Molecular parameters of 12 crude oil samples indicate a shaly source rock deposited in a marine/brackish environment. Salinity stratification, causing the development of oxygen-depleted conditions, is likely. The organic matter is dominated by aquatic biomass, including algae, dinoflagellates and chemoautotrophic bacteria. Minor angiosperm-dominated organic matter was transported into the basin from the shoreline. Specific V-shaped compound-specific carbon isotope patterns of *n*-alkanes observed in crude oils and extracts from the Tard Clay prove the dominant source rock. Minor differences between biomarker ratios are related to vertical and lateral facies variations within the Tard Clay Formation. The accumulated oils are slightly more mature than the Tard Clay in borehole W–12.

1. Introduction

During the Palaeogene, the closure of the Mesozoic Tethyan basin and subsequent basin isolation caused the birth of the Paratethys Sea (Schulz et al., 2005). The process resulted in water masses with varying salinity and redox conditions favouring the accumulation of organic matter-rich rocks (Popov et al., 2001, 2004; Rögl, 1999; Sachsenhofer et al., 2018a, 2018b). The Paratethys basin system has been subdivided into three parts because of diachronous geotectonic events: (i) the Western Paratethys, formed by the Rhône Basin and Alpine Foreland Basin, west of Munich, (ii) the Central Paratethys, composed by the remaining Alpine Foreland Basin, Carpathian Basin and Hungarian Palaeogene Basin and (iii) the larger Eastern Paratethys (Popov et al., 2004).

The Neogene Pannonian Basin formed part of the Central Paratethys and is underlain by Eocene and Oligocene sediments of the Hungarian Palaeogene Basin (Fig. 1; Tari et al., 1993). Fine-grained, organic matter-rich sediments within the Eocene and Oligocene succession were recognized as potential source rocks (e.g. Badics and Vető, 2012; Bechtel et al., 2012; Brukner-Wein et al., 1990; Körmös et al., 2020; Milota et al., 1995). Whereas it is widely accepted that the Lower Oligocene Tard Clay Formation provides the most important source rocks (Fig. 2; Bechtel et al., 2012; Brukner-Wein et al., 1990; Hertelendi and Vető, 1991; Milota et al., 1995), the Middle Eocene Kosd Formation (Körmös et al.,

* Corresponding author. University of Szeged, Department of Mineralogy, Geochemistry and Petrology, Egyetem u. 2, H-6722, Szeged, Hungary.
E-mail address: sandor.kormos@geo.u-szeged.hu (S. Körmös).

https://doi.org/10.1016/j.marpetgeo.2021.104955
Received 31 October 2020; Received in revised form 21 January 2021; Accepted 31 January 2021
Available online 5 February 2021

2020), Late Eocene Buda Marl Formation (Sachsenhofer et al., 2018a, 2018b) and Late Oligocene Kiscell Clay Formation (Milota et al., 1995) were also considered as potential source rocks (Fig. 2). Nevertheless, comprehensive organic geochemical studies have only been performed on sediments of the Tard Clay and Kosd formations (Bechtel et al., 2012; Körmös et al., 2020), whereas in-depth investigations are still missing for the Buda Marl and Kiscell Clay formations. Furthermore, detailed analysis of crude oils and thorough oil-to-source rock correlation are also absent.

This study focuses on the central-southern part of the Hungarian Palaeogene Basin. The study aims are to advance the understanding of the petroleum system by (i) characterising the maturity and source rock potential of the Upper Eocene (Kosd and Buda Marl formations) and Lower Oligocene (Tard Clay and Kiscell Clay formations) succession, (ii) determining the source rock facies of crude oils produced in several oil fields in the Hungarian Palaeogene Basin, and (iii) correlating these crude oils to a specific source rock formation.

Maturity and source rock potential of the Palaeogene succession are assessed using numerous Rock-Eval data from deep boreholes W–1, W–9 and W–12 (for location see Fig. 1b). Biomarker data of 12 crude oil samples are applied to reconstruct the depositional environment of their source rocks. Oil-to-source rock correlation is based on biomarker and compound-specific isotope data from oil samples, which are compared with new source rock data and source rock data published by Bechtel et al. (2012) and Körmös et al. (2020), who discussed the origin of the source organic matter, established on biomarker parameters, in the Tard Clay and Kosd formations, respectively.

2. Geological setting

The study area is located in the southern part of the central Hungarian Palaeogene Basin (Fig. 1), which overlies a basement constructed of the Mid-Hungarian Zone (Kovács and Haas, 2010). The Hungarian Palaeogene Basin is interpreted as a retro-arc flexural foreland basin, where the depositional facies migrated towards the ENE according to the present position (Fig. 2; Tari et al., 1993; Kováč et al., 2016). The

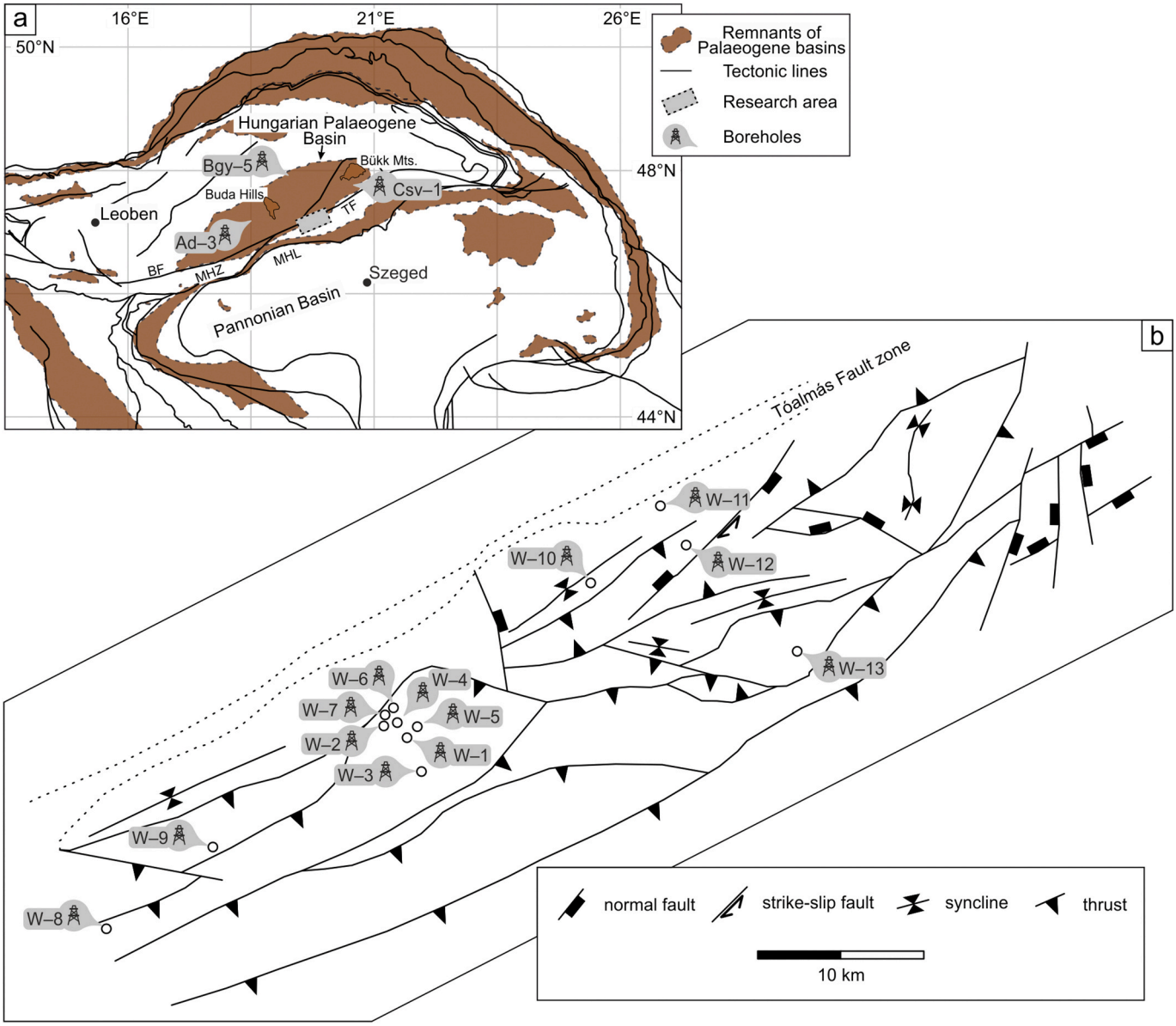

Fig. 1. Regional setting of a) the Hungarian Palaeogene Basin and b) the study area (modified after Kováč et al., 2016; Ozsvárt et al., 2016; Palotai, 2013; Schmid et al., 2008). BF – Balaton Fault, MHZ – Mid-Hungarian Zone, MHL – Mid-Hungarian Line, TF – Tóalmás Fault, Ad–3 – Alcsútdoboz–3, Bgy–5 – Balassagyarmat–5, Csv–1 – Cserépváralja–1, W–1 to W–13 are studied boreholes.

tectonic evolution has been related to normal faulting and strike-slip regimes (Palotai, 2013 and references therein). The term Palaeogene Basin comprises all sedimentary sequences, forming a single cycle from the Eocene to the Early Ottnangian (Fig. 2; Sztanó and Tari, 1993).

The Alpine Orogeny resulted in the exhumation of the Mesozoic strata during the Late Cretaceous. Subaerial exposure caused continental denudation until the Late Eocene (Haas and Kovács, 2012). The Palaeogene sediments unconformably overlie the Mesozoic basement. The sedimentary succession starts with a terrigenous basal conglomerate, breccia and variegated clay (Bauer et al., 2016; Bauer and M.Tóth, 2017). The Kosd Formation reflects a continuous upward transition to a lagoonal environment (Gidai, 1978; Less, 2005), showing the first sign of the Priabonian transgression (Báldi and Báldi-Beke, 1985). The upper part of the Kosd Formation is coal-bearing and includes pelitic sediments with varying carbonate content (Gidai, 1978; Less, 2005; Körmös et al., 2020). The Kosd Formation is overlain by the shelf deposits of the Szépvölgy Limestone Formation (Kázmér, 1985). Continued subsidence caused the deposition of the Buda Marl Formation across the Eocene-Oligocene transition, which contains marl and calcareous marl, allodapic limestones and calcareous turbidites deposited in low-oxic environments (Less, 2005; Nagymarosy and Báldi-Beke, 1988; Ozsvárt et al., 2016).

The Buda Marl Formation is overlain by the Tard Clay Formation. This formation accumulated in a euxinic basin, which was filled from the west (according to the present position; Fodor et al., 1994) by a prograding siliciclastic delta. Hence, the Tard Clay Formation is missing in the west of the Buda Hills. The Tard Clay Formation includes laminated and non-laminated shale and sandstone (Brukner-Wein et al., 1990). The degree of lamination varies considerably within the formation but is often the highest in its middle part, representing the nannozone NP23 (Nagymarosy, 1983), where dark grey siltstone alternates with white coccolith layers. These intervals are characterised by high TOC contents (max. 5 wt% TOC; Brukner-Wein et al., 1990) and represent oxygen-depleted conditions (Báldi, 1984; Bechtel et al., 2012). The overlying Kiscell Clay Formation is accumulated in a deep bathyal, well-oxygenated depositional environment (Báldi and Báldi-Beke, 1985), comprising intercalated siltstones and turbiditic sandstone bodies (Less, 2005; Milota et al., 1995).

The Palaeogene succession is terminated by interfingering heteropic sediments, including, from west (Buda Hills) to east (Bükk Mts.) the shallow sublittoral Törökbálint Sandstone Formation, the deep sublittoral–shallow bathyal Szécsény Schlier Formation and the deep sublittoral Eger Formation (Kercsmár et al., 2015). The littoral–sublittoral Budafok Formation covers the Törökbálint Sandstone, which is laterally intercalating with the upper part of the Szécsény Schlier Formation (Sztanó and Tari, 1993). The latter grades eastwards into the shallow marine Pétervására Sandstone Formation, composed of several coast parallel facies units (Sztanó and Tari, 1993). Gradual uplift in late Eggenburgian time resulted in subaerial exposure and the deposition of the Zagyvapátfalva Formation in a coastal plain setting. The Gyulakeszi Rhyolite Tuff covers the eroded surface of the Palaeogene to Eggenburgian formations (Nagymarosy, 2013). The sedimentary sequence of the Hungarian Palaeogene Basin is covered by thick Neogene sediments.

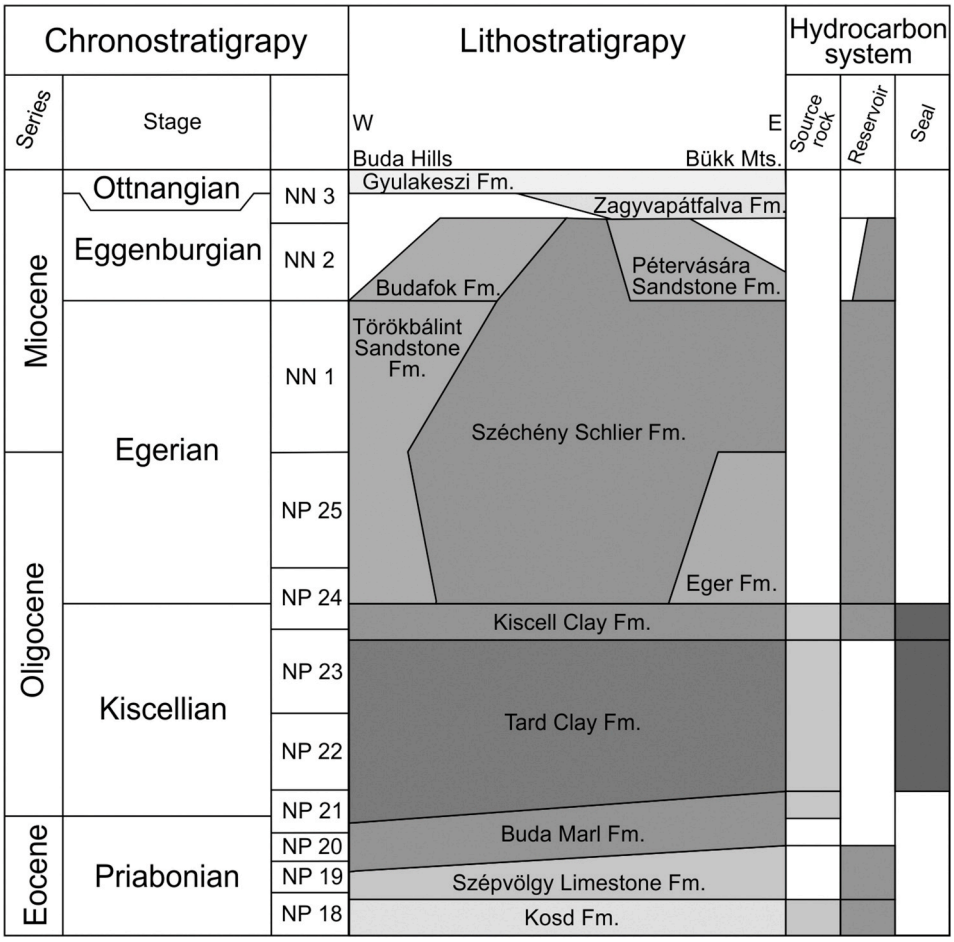

Fig. 2. Simplified lithostratigraphy of the sedimentary succession in the Hungarian Palaeogene Basin and elements of the hydrocarbon system in the study area (after Kercsmár et al., 2015; Less, 2015 oral communication; Tari et al., 1993). The nannoplankton zonation is based on Less (2005), Ozsvárt et al. (2016) and Tari et al. (1993).

2.1. Source potential of the Palaeogene sediments

Whereas the Tard Clay Formation is the most widely accepted potential source rock in the Hungarian Palaeogene Basin, organic matter rich intervals in the Buda Marl and Kiscell Clay formations were also considered (Badics and Vető, 2012; Sachsenhofer et al., 2018a, 2018b). Recently, Körmös et al. (2020) investigated the hydrocarbon potential of the coal-bearing Kosd Formation.

The Eocene Kosd Formation includes an up to 36-m-thick coal horizon. The coaly layers accumulated in a marine delta and are intercalating with siltstone containing miliolid foraminifers. The high volatile bituminous coal and coaly shale are characterised by HI values between 200 and 300 mg HC/g TOC in the deep well W–1. The coal measure is gas- and oil-prone and have reached the rank threshold for the first gas generation (Körmös et al., 2020).

The TOC contents of the Buda Marl Formation are generally below 1 wt% (max. 2.3 wt%), and HI values (<150 mg HC/g TOC) fall within the range of type III and type IV kerogen (Bechtel et al., 2012; Sachsenhofer et al., 2018a, 2018b).

The non-to weakly-laminated lower section of the Tard Clay Formation contains TOC contents up to 5 wt% (Brukner-Wein et al., 1990) but with low HI values (<185 mg HC/g TOC; Bechtel et al., 2012). Higher HI values (up to 440 mg HC/g TOC) occur in the strongly-laminated middle part of the formation, deposited in a brackish environment during the Solenovian Event (Bechtel et al., 2012; Brukner-Wein et al., 1990; Hertelendi and Vető, 1991). The upper part of the Tard Clay is characterised by gradually declining TOC and HI values (down to 0.5 wt% TOC and 75 mg HC/g TOC, respectively) with rising salinity in the water column (Bechtel et al., 2012).

The Kiscell Clay is characterised by low TOC and HI values (<1 wt% and <200 mg HC/g TOC, respectively; Milota et al., 1995) but published data are scarce.

2.2. Hydrocarbon reservoirs and traps in the study area

Hydrocarbons were detected in the fractured and weathered Mesozoic basement rocks in the research area. The basal conglomerate and breccia and the sandstone sequence of the Kosd Formation also form reservoirs and host substantial amounts of hydrocarbons. The karstified Szépvölgy Limestone and turbidite sandstone bodies within the Kiscell Clay Formation and the clastic sediments of the Miocene formations also serve as targets of exploration activities (Bauer and M.Tóth, 2017; Dolton, 2006). Various structural, stratigraphic and combination trap types were discovered within the study area. Compactional anticlines occur over basement highs. Fault-closed features, associated roll-overs and closures in flower structures are also common (Kokai, 1994; Dolton, 2006).

3. Samples and analytical methods

3.1. Samples

This study is based on rock and oil samples from boreholes W–1 to W–13, drilled by MOL Plc. during the last decades (for location see Fig. 1b). Twenty-four drill core samples, representing the Kosd Formation and Tard Clay Formation were sampled from wells W–1 and W–12. Drill cores are complemented by 196 cuttings, washed and wet samples, containing Palaeogene sediments from boreholes W–1, W–9, and W–12 provided by MOL Plc. The wells were drilled using water-based mud and were selected because of the systematically performed lag-time checks for accurate depth readings for taking drill cuttings. Intervals containing lost circulation materials and mud additives (e.g. nutshells, lignite) were avoided whenever it was possible, otherwise handpicking of solid contaminants and cavings was achieved before analysis. Moreover, sections with observed crude oil indications on the shale shakers were not considered for sampling. The organic geochemical data of core samples from the Kosd Formation were described recently by Körmös et al. (2020).

Crude oil samples were obtained from Triassic, Eocene and Oligocene reservoirs from W–1 to W–3, W–8 and W–10 to W–13 wells. MOL Plc provided additional results for oil from boreholes W–4 to W–7. The reservoirs are characterised by hydrostatic pressure (Boncz, 2004, 2013; Kiss, 1999). Table 1 lists the age and lithology of the reservoir rocks and depth of the oil-water contact.

The study is also supplemented by results acquired during investigating the Tard Clay Formation by Bechtel et al. (2012) at Alcsútdoboz–3, Cserépváralja–1 and Balassagyarmat–5 (Ad–3, Csv–1 and Bgy–5, respectively; for location see Fig. 1a).

3.2. Organic geochemical analyses

The total organic carbon (TOC) contents and Rock-Eval parameters of cutting and core samples were determined in the laboratories of MOL and Montanuniversität Leoben, respectively. An ELTRA Helios CS-580A analyser was used to obtain the TOC contents on duplicates of powdered core samples, pre-treated by H_3PO_4, by combustion. The TOC contents of cutting samples were determined by Rock-Eval pyrolysis on duplicates of pulverized samples. The TOC contents achieved by pyrolysis of bulk rocks (Rock-Eval 6) and by combustion of samples, pre-treated by acid (ELTRA), agree very well (cf. Behar et al., 2001). Rock-Eval 6 instruments (Lafargue et al., 1998) were employed to quantify the free and generated hydrocarbons (S1 and S2 peaks, respectively) in both laboratories. The temperature at the maximum hydrocarbon generation (Tmax [°C]) was detected and applied as a maturity indicator. Derived Rock-Eval parameters include the hydrogen index (HI = S2 × 100/TOC [mg HC/g TOC]), the production index (PI = S1/(S1 + S2) [—]; Espitalié et al., 1977) and the petroleum potential (PP = S1 + S2 [mg HC/g rock]).

Aliquots of powdered rock samples, 10 g each, were extracted using dichloromethane solvent at 75 °C and 110 bar over 1 h utilizing a Dionex ASE 350 accelerated solvent extractor. The elemental sulphur content of the solution was removed by adding copper. The extracts were concentrated to 1 ml solution by a Zymark TurboVap 500 closed cell concentrator. The crude oil samples, 50 mg each, and the concentrated extracts were diluted by a mixture of hexane–dichloromethane (80:1)

Table 1
Age, lithology and depth of the oil-water contact for reservoirs of studied oil samples (after Boncz, 2004, 2013 and Kiss, 1999).

Well name	Age	Lithology	Oil-water contact [m; MD]
W–1	Eocene	Sandstone, polymict conglomerate	2469
W–2	Eocene and Triassic	Sandstone, polymict conglomerate and limestone	2513
W–3	Eocene	Sandstone, polymict conglomerate	2490
W–4	Eocene and Triassic	Sandstone, polymict conglomerate and limestone	2453
W–5	Eocene	Sandstone, polymict conglomerate	2495
W–6	Eocene	Sandstone, polymict conglomerate	2510
W–7	Eocene	Sandstone, polymict conglomerate	2449
W–8	Eocene	Limestone breccia	1722
W–10	Eocene and Triassic	Fractured- and karstified limestone	1780
W–11	Jurassic	Limestone	2491
W–12	Oligocene and Eocene	Fractured siltstone and biogenic limestone	2316
W–13	Triassic	Fractured limestone	2249

MD – measured depth.

solution and insoluble asphaltenes were precipitated, and separated by centrifugation. Hexane diluted and dissolved the maltenes, which were injected into a Margot Köhnen-Willsch medium-pressure liquid chromatography instrument to separate the NSO (containing nitrogen, sulphur and oxygen), saturated and aromatic compounds (Radke et al., 1980b). The saturated and aromatic compounds were concentrated and internal standards were added (deuterated *n*-tetracosane and 1, 1′-binaphthyl, respectively). The normal and branched–cyclic alkanes were further separated for compound-specific isotope analyses using an improved 5 Å molecular sieve method (Grice et al., 2008). The isotope fractionation of compounds seems unlikely based on the low-temperature-controlled chemical reactions during sample preparation.

The saturated hydrocarbon fractions were analysed using a Thermo Scientific TraceGC gas chromatograph attached to a flame ionisation detector, installed with an HP-PONA fused silica capillary column (50 m, i.d. 0.2 mm; 0.5 μm film thickness). The samples were injected in split mode at 270 °C. The oven temperature was programmed to an initial 5 min period at 32 °C, followed by 2.5 °C/min heating rate to 310 °C and hold for 30 min. Helium was used as the carrier gas. The flame ionisation detector was operated at 320 °C with 350 and 35 ml/min flow rates of air and hydrogen, respectively. Data were processed using an Xcalibur data system. Individual compounds were identified based on retention time. The concentration of *n*-alkanes and acyclic isoprenoids, as well as the corresponding concentration ratios, are based on peak area integration compared to the internal standard.

A gas chromatograph coupled to a ThermoFisher ISQ mass spectrometer equipped with a DB-5MS fused silica capillary column (60 m, i.d. 0.25 mm; 0.25 μm film thickness) was used to analyse the saturated and aromatic hydrocarbon fractions. The oven temperature was programmed to an initial 70 °C and raised to 300 °C at 4 °C/min rate, followed by an isothermal period of 15 min. The carrier gas was helium. The samples were injected through an injector at 275 °C in splitless mode. Electron ionisation of the molecular species was achieved over a scan range of 50–600 m/z with a total scan time of 500 msec during the analyses. Data were processed using an Xcalibur data system. Individual compounds were identified in the total ion current (TIC) chromatogram based on retention time and fragment ions of m/z 191, 217, 218, 231, and 259 were chosen for recognition of hopanoids and steranes (Ensminger et al., 1978; Summons et al., 1987; Wingert and Pomerantz, 1986), as well as the mass spectra were compared with published data. The 4-methylsteranes were distinguished on the diagnostic ion, m/z 231 mass chromatograms, and 24–*n*–propylcholestanes were determined according to the registered mass spectra (Moldowan et al., 1990). Absolute concentrations and relative percentages of different compound groups were estimated using peak areas of internal standards in the TIC chromatograms, or by integrating peak areas in convenient mass chromatograms employing response factors to quantify the total ion abundance.

Stable carbon isotope measurements of *n*-alkanes were performed on selected samples, including crude oils and rock extracts from drill cores, using a Trace GC instrument coupled to a ThermoFisher DELTA-V IR mass spectrometer *via* a GC isolink combustion interface. CO_2 was injected during each analysis as monitoring gas. The GC column and temperature programme used were the same as above. The saturated and aromatic hydrocarbon fractions of selected crude oils and rock extracts from drill cuttings were placed into tinfoil boats for the bulk carbon isotope analyses and combusted in an oxygen atmosphere using an elemental analyser (Flash EA 1112) at 1020 °C. The evolving CO_2 was separated by column chromatography and analysed online using a DELTA-V IR-MS. The $^{13}C/^{12}C$ isotope ratios of CO_2 were compared with the monitoring gas. Stable isotope ratios are expressed relative to the Vienna Pee Dee Belemnite (V-PDB) standard in delta notation ($\delta^{13}C = [(\delta^{13}C/\delta^{12}C)_{sample}/(\delta^{13}C/\delta^{12}C)_{standard} - 1]$; Coplen, 2011). Delta notation is reported in parts per thousand or per mil (‰). The analytical error during the measurements was better than 0.2‰.

4. Results

4.1. Bulk geochemical parameters of source rocks

Several wells, including W–1, W–9 and W–12, penetrated the potential source rocks, which were sampled for hydrocarbon generation potential assessment (Fig. 3). Rock-Eval data are compiled in Appendices A (W–1), B (W–9) and C (W–12). The assignment of the sediments to stratigraphic units follows the internal reports of MOL Plc.

The Kosd Formation was penetrated by wells W–1 and W–9. TOC contents in samples from the Kosd Formation vary widely from 0.10 to 78.39 wt%, reflecting the presence of different lithotypes, including organic matter-lean siltstone, claystone, coaly shale and coal. The Tmax and HI values range from 431 to 451 °C and from 31 to 348 mg HC/g TOC, respectively (Fig. 4a). The PP varies between 0.05 and 209.64 mg HC/g rock and averages at 52.09 mg HC/g rock in high TOC (>2 wt%) intervals.

The sediments of Buda Marl Formation in wells W–1, W–9 and W–12 are characterised by TOC contents ranging from 0.04 to 2.65 wt% (avg. 0.73 wt%). The Tmax values range from 430 to 444 °C and the HI varies from 33 to 325 mg HC/g TOC (Fig. 4b). The PP reaches a maximum of 10.55 mg HC/g rock in well W–9 and averages at 4.78 mg HC/g rock at intervals where the TOC content is greater than 1 wt%.

Significant differences exist between organic matter contents and HI values of the Tard Clay Formation in the western well W–9 (0.15–0.30 wt% TOC; 65–104 mg HC/g TOC) and the eastern well W–12 (0.80–1.89 wt% TOC; 189–439 mg HC/g TOC). The Tmax values range from 434 to 441 °C (Fig. 4c). The PP is between 1.94 and 9.31 mg HC/g rock in well W–12 and averages at 6.14 mg HC/g rock in the upper high TOC (>1 wt %) interval.

The TOC contents of the Kiscell Clay Formation in wells W–1, W–9 and W–12 range from 0.16 to 0.71 wt% (avg. 0.45 wt%). The Tmax values vary from 419 to 439 °C and the HI values are between 55 and 327 mg HC/g TOC (Fig. 4d). The PP is generally below 1 mg HC/g rock (max. 1.44 mg HC/g rock).

4.2. Crude oils

Crude oil samples from different hydrocarbon accumulations in the study area were analysed. Reservoir rocks include Mesozoic fractured carbonates, Eocene karstified carbonates, Eocene and Oligocene clastic reservoirs (Table 1). Eight samples were analysed in this study (W–1o to W–3o and W–8o to W–13o; Table 2), whereas MOL Plc provided data of the samples W–4o to W–7o (Table 2).

4.2.1. Molecular composition

The saturated hydrocarbons dominate in the oil samples, except in W–3o and W–11o. In the latter, the polar fractions prevail over the hydrocarbons (Table 2). The NSO compounds also appear in greater proportion in W–1o, W–8o, W–12o and W–13o samples, whereas the aromatic and asphaltene fractions remain constant in most samples (Table 2).

4.2.1.1. Straight-chain alkanes and isoprenoids. The *n*-alkanes dominate the aliphatic fraction of the crude oils (Fig. 5a). Short-chain *n*-alkanes (n-$C_{15–19}$) are typically slightly more abundant than mid-chain *n*-alkanes (n-$C_{21–25}$), but mid-chain *n*-alkanes predominate in samples W–8o, W–10o and W–13o (Table 2). Long-chain *n*-alkanes (n-$C_{27–31}$) are also abundant in samples W–8o, W–10o and W–13o (Table 2). No distinct odd-over-even carbon number preference exists; the CPI values are close to one (max. 1.12; Table 2). Acyclic isoprenoids ($C_{13–20}$) are considerably abundant (Fig. 5a). Pristane dominates over phytane (Fig. 5a; Table 2). The Pr/n-C_{17} (0.82–1.01) and Ph/n-C_{18} (0.43–0.56) ratios are similar in most oils but significantly lower in samples W–12o and W–13o (0.64–0.68 and 0.38–0.39, respectively; Fig. 6; Table 2).

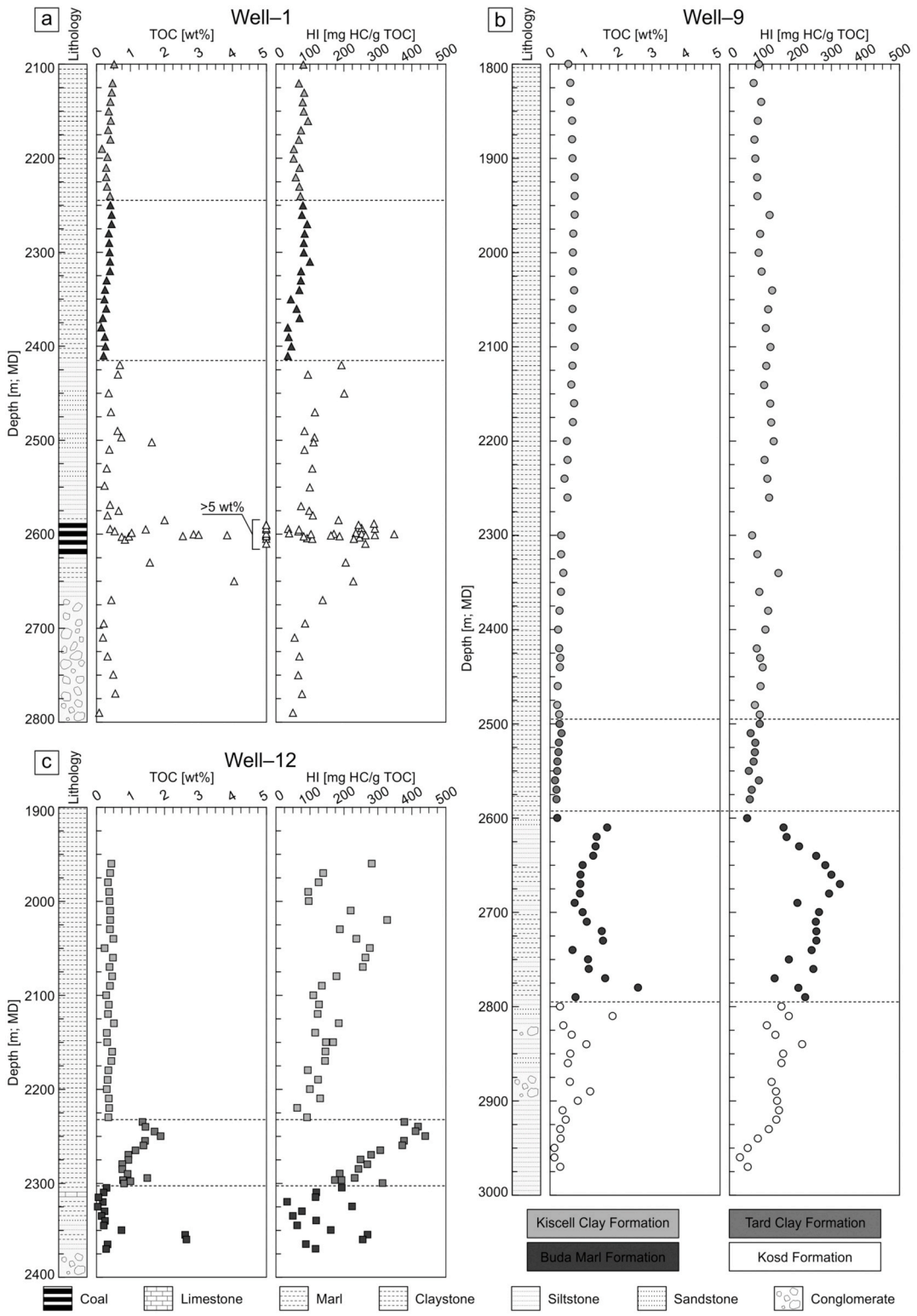

Fig. 3. Organic geochemical depth logs of the a) W–1, b) W–9 and c) W–12 wells based on Appendices A, B and C. The simplified lithologies presented according to the description of drill cuttings for each well. MD – measured depth.

4.2.1.2. Steroids. The C_{27}–C_{29} 5α,14β,17β (H) and 5α,14α,17α(H) sterane isomers are present in the crude oils (Fig. 7a). Normalised values of ααα(20R) steranes are provided on a ternary diagram (Huang and Meinshein, 1979), used to assess the depositional facies of organic matter (Fig. 8). The C_{28} and C_{29} homologues show a slight prevalence and are present in similar percentages (C_{28}/C_{29}: avg. 0.98; Fig. 8; Table 2). The 24-*n*-propylcholestane and C_{28}–C_{30} homologues of the 4–methylsteranes are also identified in significant amounts (Fig. 7a). Diasteranes occur in lower concentration than the regular steranes (Fig. 7a) but show similar carbon number distribution. The values of the C_{27} diasteranes relative to the C_{27} regular steranes (C_{27} diaS/(diaS + regS)) vary from 0.19 to 0.49 (avg. 0.28; Table 2). Pregnanes are also present in the samples and the C_{21}–C_{22} homologues show prominent peaks in most oil samples (Fig. 7a). The ratio of pregnanes to regular

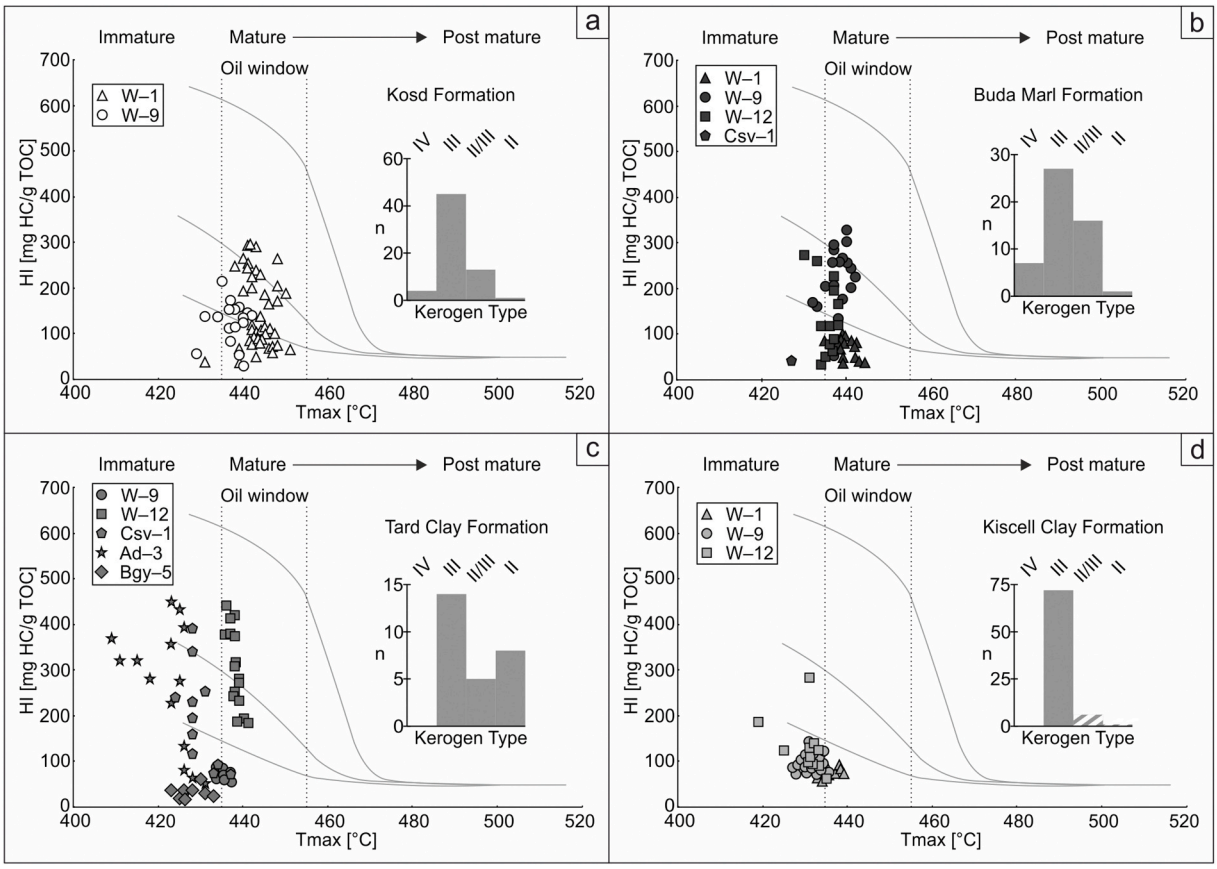

Fig. 4. Hydrocarbon generation potential assessment of a) Kosd Formation, b) Buda Marl Formation, c) Tard Clay Formation and d) Kiscell Clay Formation. Results presented for Csv–1, Ad–3 and Bgy–5 boreholes are taken form Bechtel et al. (2012). The hatched columns of the frequency diagram in Fig. 4d represent kerogen types without recorded Tmax values.

Table 2
Percentage of extracted fractions and concentration ratios of selected compounds and compound groups within the hydrocarbon fractions of the crude oil samples.

ID	a	b	c	d	e	f	g	h	i	j	k	l	m	n	o	p	q	r	s	t	u
#	[wt%]				[‰; V-PDB]		[%]							[%]								
W–1o	55	16	26	3	n.d.	n.d.	36	33	17	1.06	0.96	0.54	1.79	23	42	35	1.20	0.16	0.22	0.51	0.74
W–2o	72	13	10	4	n.d.	n.d.	35	33	16	1.05	0.89	0.48	1.83	26	40	34	1.18	0.23	0.26	0.56	0.74
W–3o	19	4	74	4	n.d.	n.d.	35	33	17	1.00	0.88	0.50	1.78	24	40	36	1.11	0.20	0.23	0.52	0.75
W–4o	77	10	7	6	−27.7	−26.3	36	31	18	1.03	0.86	0.47	2.01	29	33	38	0.87	n.d.	0.24	0.52	0.68
W–5o	79	11	3	7	−27.8	−26.6	36	31	18	1.02	0.86	0.48	1.96	30	34	36	0.94	n.d.	0.22	0.53	0.69
W–6o	79	11	3	8	−27.4	−26.5	36	31	18	1.03	0.84	0.48	1.96	29	33	38	0.87	n.d.	0.24	0.54	0.69
W–7o	80	11	2	8	−27.7	−26.6	36	31	18	1.05	0.93	0.51	2.04	29	33	38	0.87	n.d.	0.22	0.53	0.69
W–8o	45	14	34	7	n.d.	n.d.	27	34	27	1.05	0.82	0.55	1.66	35	30	35	0.86	0.02	0.36	0.52	0.80
W–10o	70	12	11	7	n.d.	n.d.	18	34	35	1.12	0.92	0.43	2.19	27	32	40	0.80	0.04	0.42	0.51	0.62
W–11o	28	12	58	3	n.d.	n.d.	35	33	17	1.01	1.01	0.56	1.77	23	40	36	1.11	0.16	0.19	0.50	0.71
W–12o	60	10	26	4	n.d.	n.d.	39	31	15	1.06	0.68	0.38	1.91	24	38	38	1.00	0.11	0.31	0.56	0.67
W–13o	56	10	32	3	n.d.	n.d.	27	33	28	1.06	0.64	0.39	1.68	34	32	35	0.91	0.10	0.49	0.51	0.77

a – saturated hydrocarbons, b – aromatic hydrocarbons, c – polar compounds, d – asphaltenes, e – $\delta^{13}C$ saturated hydrocarbons, f – $\delta^{13}C$ aromatic hydrocarbons, g – *n*-C_{15-19}/*n*-C_{15-33}, h – *n*-C_{21-25}/*n*-C_{15-33}, i – *n*-C_{27-31}/*n*-C_{15-33}, j – CPI (Bray and Evans, 1961), k – Pr/*n*-C_{17}, l – Ph/*n*-C_{18}, m – Pr/Ph, n – ααα(20R) C_{27} steranes/Σ ααα(20R) regular steranes, o – ααα(20R) C_{28} steranes/Σ ααα(20R) regular steranes, p – ααα(20R) C_{29} steranes/Σ ααα(20R) regular steranes, q – C_{28}/C_{29} ααα(20R) steranes, r – C_{21-22}/C_{27-29} steranes, s – C_{27} diaS/(diaS + regS), t – 20S/(20S + 20R) ααα C_{29} sterane, u – αββ/(αββ+ααα) C_{29} sterane.

steranes (C_{21-22}/C_{27-29}) reaches a maximum of 0.23 (avg. 0.13; Table 2). The stereoisomer ratios of αααC$_{29}$ steranes range from 0.50 to 0.56 (avg. 0.52) and the ratios of αββ/(αββ+ααα) isomers vary from 0.62 to 0.80 (avg. 0.72; Table 2).

4.2.1.3. Terpenoids. The occurrence of C_{27} to C_{35} 17α,21β(H)–type hopanes dominates the hopanoids pattern with the absence of C_{28} hopanes. The predominant hopanoid in most samples is 17α,21β–C_{30} hopane (H; Fig. 7b). The 17α,21β(H)–type homohopanes show an exponentially decreasing pattern in peak height with increasing carbon numbers (Fig. 7b). The 18α(H)–oleanane (Ol) is also present in considerable concentration (Fig. 7b). A series of C_{19}– to C_{29}– tricyclic terpanes (TT) appears. Whereas C_{22}TT and C_{27}TT are absent, a slight dominance of C_{23}TT occurs (Fig. 7b), also reflected by low C_{19}/C_{23}TT, C_{20}/C_{23}TT, C_{21}/C_{23}TT and C_{24}/C_{23}TT ratios (avg. 0.55, 0.59, 0.83, 0.68, respectively; Table 3). The C_{24} tetracyclic terpane (TeT) and degraded TeT (10β(H)–des–A–oleanane and 10β(H)–des–A–lupane) are also identified in the samples (Fig. 7b). Gammacerane is present in low concentrations

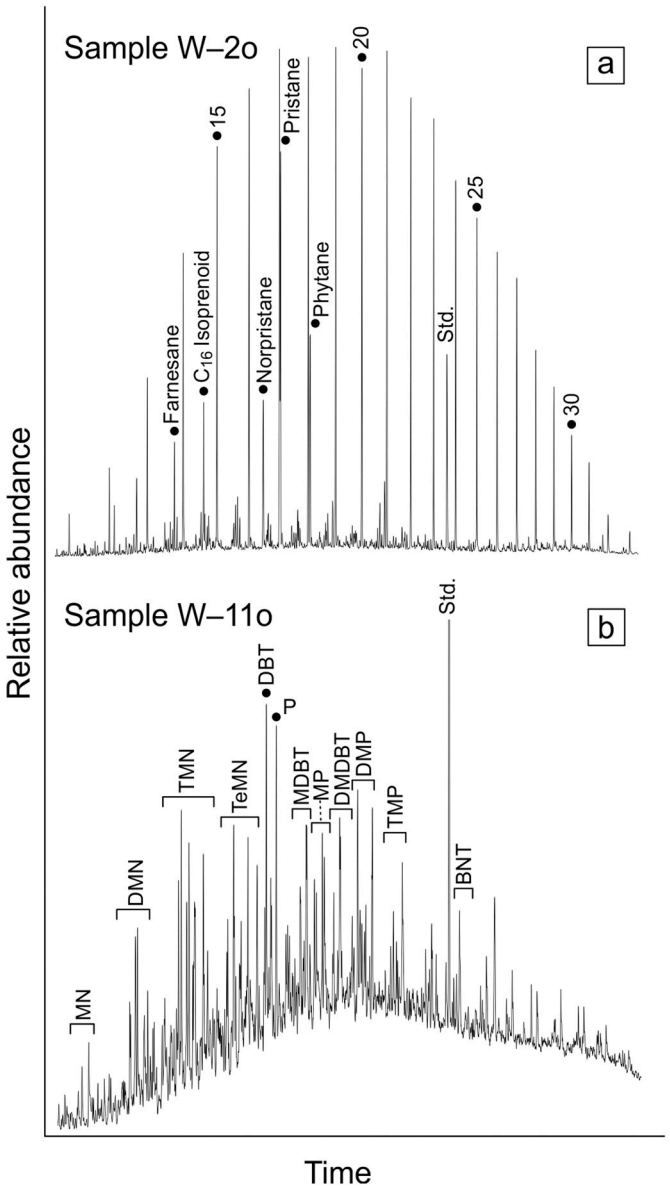

Fig. 5. Gas chromatograms (total ion current) of the (a) saturated and (b) aromatic hydrocarbon fractions. *n*-Alkanes are labelled according to the carbon number. MN – methylnapthalenes, DMN – dimethylnapthalenes, TMN – trimethylnapthalenes, TeMN – tetramethylnapthalenes, P – phenanthrene, MP – methylphenanthrenen, DMP – dimethyphenanthrene, TMP – trimethylphenanthrene, DBT – dibenzothiophene, MDBT – methyldibenzothiophene, DMDBT – dimethyldibenzothiophene, BNT – benzonaphthothiophene, Std. – standard (deuterated *n*-tetracosane and 1,1′–binaphthyl, respectively).

(Fig. 7b). The source-related biomarker ratios are similar in most of the analysed crude oils (Table 3). The stereoisomer ratio 22S/(22S + 22R) of 17α,21β(H)–C_{32} hopanes varies from 0.55 to 0.61 (avg. 0.58; Table 3).

4.2.1.4. Aromatic hydrocarbons. The aromatic hydrocarbon fractions of the crude oils are characterised by the occurrence of naphthalene, phenanthrene, dibenzothiophene and their alkylated counterparts (Fig. 7b). Benzonaphthothiophenes are also present at a higher concentration in the samples (Fig. 7b).

Vitrinite reflectance values based on the methylphenanthrene index (MPI 1; Radke et al., 1982a; 1982b) vary between 0.75 and 0.96% $Rc_{(MPI\ 1)}$ (avg. 0.84% $Rc_{(MPI\ 1)}$; Table 3; Radke and Welte, 1983). The dibenzothiophene/phenanthrene ratios (DBT/P; Hughes et al., 1995) range from 0.22 to 1.27 (avg. 0.66; Fig. 9; Table 3).

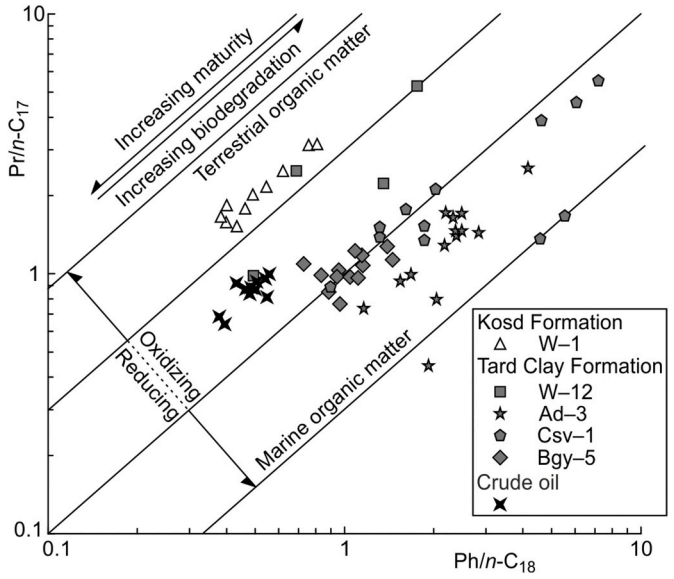

Fig. 6. Cross plot of phytane/*n*-C_{18} *vs.* pristane/*n*-C_{17} of source rock and crude oil samples (after Connan and Cassou, 1980). Results representing W–1, Ad–3, Csv–1 and Bgy–5 wells are taken from Körmös et al. (2020) and Bechtel et al. (2012).

4.2.2. Stable carbon isotope data

The stable carbon isotope composition ($\delta^{13}C$) of the saturated hydrocarbon fractions in crude oils W–4o to W–7o ranges from −27.8‰ to −27.4‰. The $\delta^{13}C$ values of the aromatic hydrocarbon fractions vary from −26.6‰ to −26.3‰ (Fig. 10a; Table 2).

Compound-specific $\delta^{13}C$ data of *n*-alkanes are plotted versus chain length in Fig. 10b. Short-chain *n*-alkanes show a trend towards lower values (enrichment in ^{12}C) with increasing chain length (Table 4). Minima occur at *n*-C_{21}, except in W–6o and W–8o, where the minima occur at *n*-C_{20}. The mid-chain *n*-alkanes (*n*-$C_{21–27}$) show an increasing trend. In contrast, long-chain *n*-alkanes (*n*-C_{27+}) exhibit slightly decreasing $\delta^{13}C$ values with an increase at *n*-C_{30} (Fig. 10b; Table 4).

5. Discussion

The study (i) assesses the petroleum potential of Upper Eocene to Lower Oligocene sediments in the Hungarian Palaeogene Basin, (ii) characterises the facies of the source rocks of the accumulated oils and (iii) correlate the accumulated oils to a specific source rock formation. Therefore, a detailed biomarker-based interpretation of the source rocks is beyond the scope of the discussion. Nevertheless, Table 5 summarises source and maturity related biomarker parameters, calculated for the Kosd and Tard Clay formations.

5.1. Hydrocarbon generation potential of the Eocene to Lower Oligocene succession

The TOC contents and Rock-Eval parameters are used to assess the remaining hydrocarbon generation potential of the investigated samples. The Kosd Formation was encountered at W–1 well with a thickness of 376 m, which includes a 36-m-thick coal measure (Körmös et al., 2020). In the W–9 well, the Kosd Formation is ~200 m thick. The HI reaches 350 mg HC/g TOC (Appendix A); however, HI values greater than 250 mg HC/g TOC are rare. The HI values of the drill cuttings suggest the presence of kerogen type IV to II/III (Peters, 1986), with a dominance of the type III kerogen (Fig. 4a). The HI values increase with increasing TOC content (Fig. 3; Appendices A and B), correlating with a previous study (Körmös et al., 2020). Tmax values are higher in W–1 well (avg. 445 °C at 2400–2800 m) than in the W–9 well (avg. 437 °C at

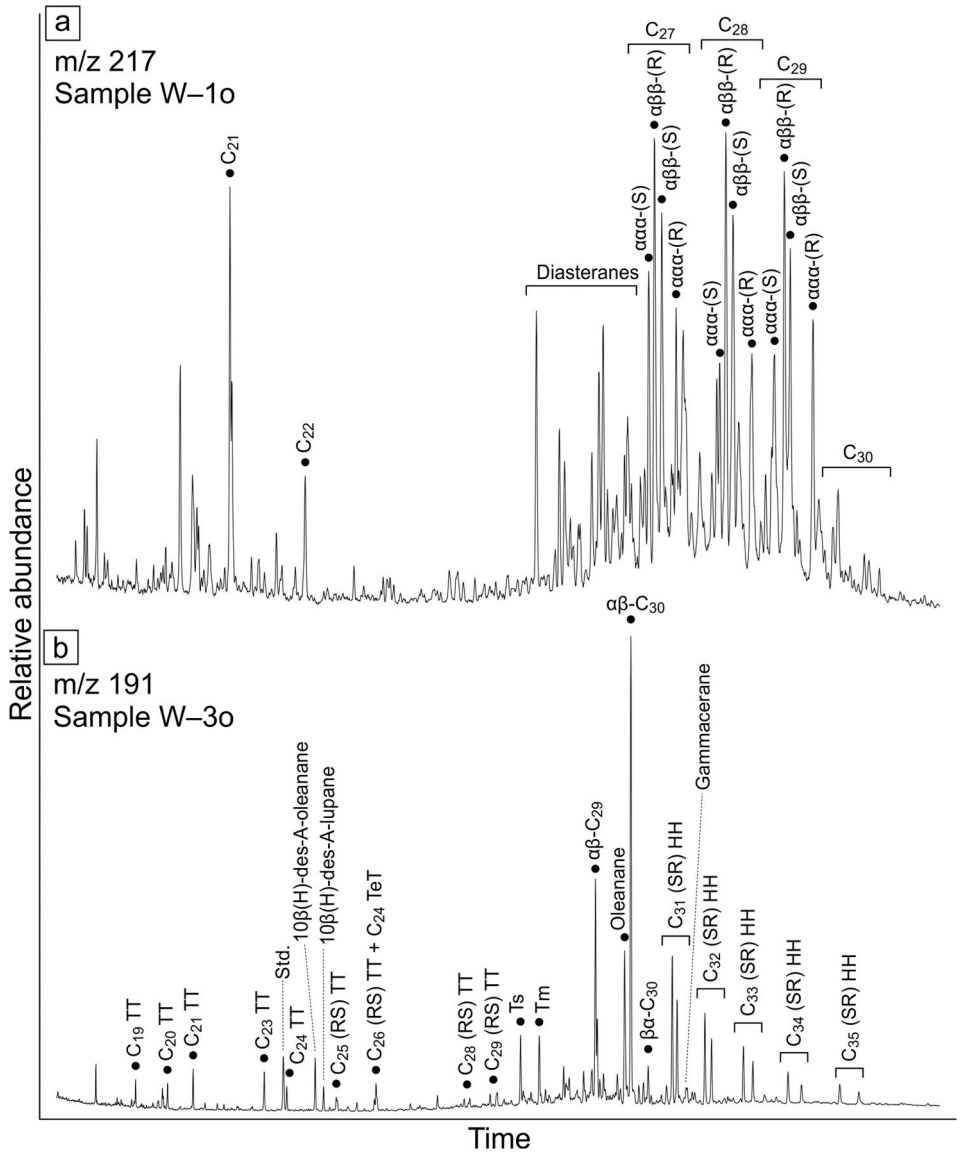

Fig. 7. Representative mass chromatograms of the a) steranes (m/z 217) and b) terpanes (m/z 191). TT – tricyclic terpane, TeT – tetracyclic terpane, HH – homohopanes, Std. – standard (deuterated *n*-tetracosane).

2800–3000 m). Nevertheless, oil window maturity (Bordenave et al., 1993) is reached in both wells. The high TOC contents and HI values point to a gas-and-oil-generating source with a very good and excellent petroleum potential (avg. 16.05 mg HC/g rock; Fig. 11a; Appendices A and B; Peters and Cassa, 1994).

The Buda Marl Formation was studied in wells W–1, W–9 and W–12. The thickness of the formation reaches a maximum of 190 m at W–9, which is thicker than reported before (e.g. Less, 2005). Bechtel et al. (2012) and Sachsenhofer et al. (2018a, 2018b) demonstrated that the uppermost part of the Buda Marl Formation, ~20 m thick, contains a maximum of 2.3 wt% TOC and HI values below 150 mg HC/g TOC at well Ad–3. Based on the obtained HI values, the kerogen type varies between type IV and II/III (Fig. 4b; Peters, 1986), whereas kerogen type III prevails. The Tmax values indicate oil window maturity in all wells (avg. 440 °C; Bordenave et al., 1993). Sediments with HI values exceeding 200 mg HC/g TOC occur in wells W–9 and W–12 and contain an average TOC of 1.25 wt%. These intervals within the Buda Marl Formation, which could reach a thickness of 100 m, are classified as fair oil source rocks with an average petroleum potential of 3.97 mg HC/g rock (Fig. 11b; Appendix B; Peters and Cassa, 1994).

The Tard Clay Formation is a well-known and exhaustively studied potential source rock (e.g. Badics and Vető, 2012; Bechtel et al., 2012; Brukner-Wein et al., 1990; Milota et al., 1995). It was studied in wells W–9 and W–12. In W–12, the Tard Clay Formation is ~70 m thick. TOC contents (0.8–1.9 wt%) and HI values (190–440 mg HC/g TOC) increase upwards. The prevalence of kerogen type II and II/III (Figs. 3 and 4c; Appendix C) agrees with previously published data from this formation (e.g. Badics and Vető, 2012; Bechtel et al., 2012; Brukner-Wein et al., 1990). The sharp decrease of TOC contents and HI values at the top of the Tard Clay Formation (Fig. 3) suggests an unconformity. Therefore, the uppermost part of the formation could be missing. In contrast to W–12, Tard Clay Formation in well W–9 (or its time-equivalent) is organic matter-lean (avg. 0.23 wt%) and contains type III kerogen. The Tmax values indicate oil window maturity in both wells (avg. 437 °C; Bordenave et al., 1993). The Tard Clay Formation in W–12 is characterised as a fair oil source with a good petroleum potential in the upper 30 m (avg. 6.47 mg HC/g rock; Fig. 11c; Appendix C; Peters and Cassa, 1994).

Based on Milota et al. (1995), the Kiscell Clay Formation could reach a thickness of 500 m and some pelitic beds within the formation have been evaluated as a fair quality source. In the studied wells, the formation is up to 690 m thick (W–9; Fig. 3; Appendix B). The TOC content

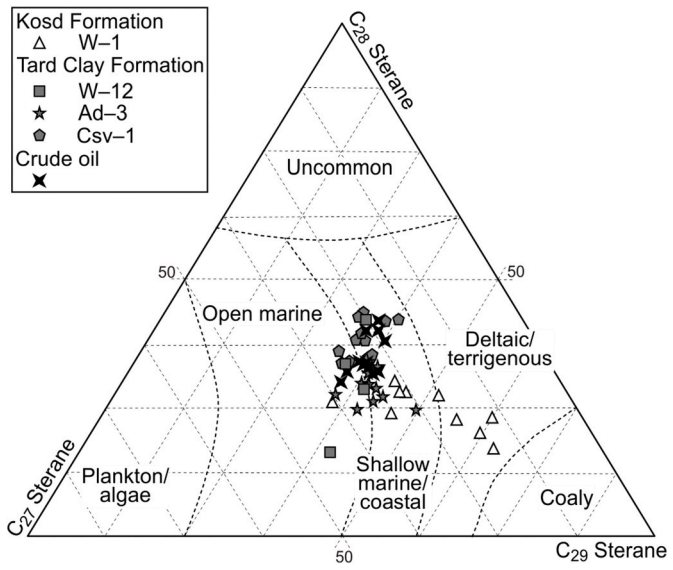

Fig. 8. Ternary plot of ααα(20R) regular steranes (after Huang and Meinshein, 1979). The normalised abundance of the regular steranes in the Tard Clay and Kosd formations from wells Ad–3, Csv–1 and W–1 are taken from Bechtel et al. (2012) and Körmös et al. (2020).

remains below 0.7 wt% (Appendices A, B and C). The HI values reveal the predominance of type III kerogen (Fig. 4d; Peters, 1986). Surprisingly, and despite low TOC contents (max. 0.51 wt%), type II/III and II kerogens occur in well W–12 between 1960 m and 2070 m depth (Appendix C). The Tmax values indicate that the organic matter is marginally matured in all wells (avg. 432 °C; Bordenave et al., 1993). The petroleum potential classifies the Kiscell Clay Formation as poor source rock (avg. 0.56 mg HC/g rock; Fig. 11d; Appendices A, B and C; Peters and Cassa, 1994).

Overall, the reviewed formations show significant variations in thickness, TOC contents and HI values. However, apart from the Kiscell Clay Formation, all formations include intervals that are capable of hydrocarbon generation.

5.2. Depositional facies of the source organic matter of oil samples

The low- and intermediate-molecular weight *n*-alkanes are present in a high and relatively constant proportion in most of the crude oils, except in W–8o, W–10o and W–13o (Fig. 5a; Table 2), representing shallow reservoirs (oil-water contact between 1722 and 2249 m depth; Table 1). The short-chain *n*-alkanes (*n*-$C_{15–19}$) were identified in algae and microorganisms (Cranwell, 1977; Cranwell et al., 1987). The $\delta^{13}C$-values of short-chain *n*-alkanes (Fig. 10b; Table 4) agree with carbon isotope values often found in freshwater algae (e.g. Lamb et al., 2006). Aquatic autotroph organisms utilise dissolved $CO_{2[AQ]}$ or HCO_3^- as the inorganic carbon source and rather take $CO_{2[AQ]}$ until the source is exhausted, which leads to ^{12}C enrichment (Lamb et al., 2006; Meyers, 1997). The concentration of $CO_{2[AQ]}$ in the water mass is the function of pH and temperature, therefore, marine organisms are characterised by heavier carbon isotope composition (Lamb et al., 2006). Nevertheless, the enzymatically mediated biological processes of bacteria are likely to lower the $\delta^{13}C$ composition of the biomass (Cloern et al., 2002), especially in oxygen-depleted conditions (Teece et al., 1999). The degradation of organic constituents of marine algae may produce similar carbon isotope composition than in the studied samples (Meyers, 1997). The mid-chain *n*-alkanes (*n*-$C_{21–25}$) were reported to predominate in extracts from aquatic macrophytes and *Sphagnum* (Bingham et al., 2010; Dehmer, 1995; Ficken et al., 2000; Nott et al., 2000). The carbon isotope composition of mid-chain *n*-alkanes does not differ greatly from the short-chain homologues (Fig. 10b; Table 4) and corresponds well to the $\delta^{13}C$-values of C3 plants (e.g. Meyers, 1997). Submerged macrophytes behave like algae in the process of inorganic carbon fixation (Lamb

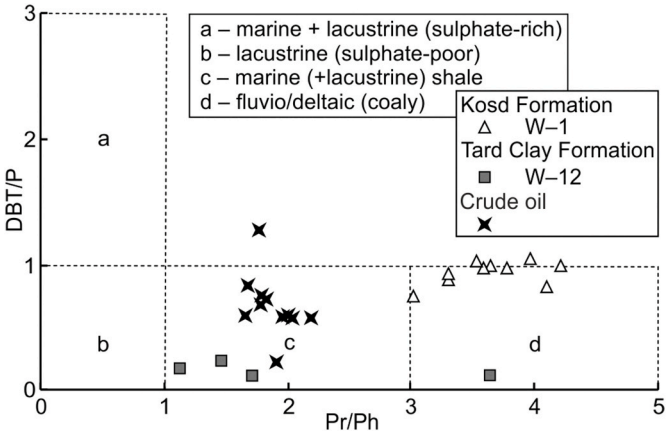

Fig. 9. Cross plot of pristane/phytane *vs.* dibenzothiophenes/phenanthrene ratios of the studied samples (after Hughes et al., 1995). The ratios in the Kosd Formation from well W–1 is taken from Körmös et al. (2020). Pr – pristane, Ph – phytane, DBT – dibenzothiophenes, P – phenanthrene.

Table 3
Source- and maturity-related biomarker and non-biomarker ratios of crude oil samples.

ID	a	b	c	d	e	f	g	h	i	j	k	l	m	n	o	p
#															[%]	
W–1o	0.56	0.57	0.83	0.57	0.93	0.07	0.30	0.46	0.25	0.68	0.09	0.31	0.57	0.51	0.81	0.75
W–2o	0.60	0.68	0.81	0.61	0.80	0.09	0.30	0.40	0.29	0.75	0.09	0.32	0.55	0.56	0.87	0.72
W–3o	0.58	0.65	0.86	0.76	0.88	0.08	0.31	0.45	0.23	0.71	0.08	0.34	0.56	0.52	0.84	0.68
W–4o	n.d.	n.d.	n.d.	0.54	0.84	0.12	0.39	0.45	0.29	0.86	0.11	0.31	0.59	0.52	0.87	0.59
W–5o	n.d.	n.d.	n.d.	0.58	0.95	0.09	0.40	0.46	0.33	0.88	0.12	0.32	0.60	0.53	0.86	0.58
W–6o	n.d.	n.d.	n.d.	0.57	0.95	0.09	0.40	0.45	0.30	0.87	0.12	0.31	0.61	0.54	0.87	0.59
W–7o	n.d.	n.d.	n.d.	0.45	1.06	0.10	0.40	0.46	0.33	0.88	0.12	0.32	0.60	0.53	0.75	0.57
W–8o	0.31	0.66	0.79	0.89	1.02	0.04	0.19	0.43	0.31	0.64	0.10	0.39	0.60	0.50	0.82	0.59
W–10o	0.65	0.77	0.72	0.86	0.77	0.04	0.19	0.49	0.31	0.90	0.10	0.41	0.58	0.49	0.87	0.55
W–11o	0.68	0.74	0.96	0.59	0.94	0.08	0.17	0.40	0.24	0.64	0.08	0.22	0.55	0.50	0.76	1.27
W–12o	0.54	0.43	0.77	0.59	0.78	0.05	0.24	0.41	0.26	0.78	0.09	0.33	0.58	0.56	0.77	0.22
W–13o	0.48	0.21	0.87	1.09	0.84	0.04	0.21	0.54	0.35	0.88	0.10	0.32	0.59	0.62	0.96	0.83

a – C_{19}/C_{23}TT, b – C_{20}/C_{23}TT, c – C_{21}/C_{23}TT, d – C_{24}/C_{23}TT, e – C_{26}/C_{25}TT, f – C_{23}TT/17α,21β–C_{30} hopane (C_{23} TT/H), g – Ol/(Ol + H); h – 17α,21β–C_{30} norhopane/17α,21β–C_{30} hopane (NH/H), i – 17α,21β–C_{31} (22R) homohopane/17α,21β–C_{30} hopane (C_{31}(R)/H), j – 17α,21β–C_{35} (22S) homohopane/17α,21β–C_{34} (22S) homohopane (C_{35}(S)/C_{34}(S)), k – 17α,21β–C_{35} homohopane/17α,21β–$C_{31–35}$ homohopane ($C_{35}/C_{31–35}$), l – steranes/hopanes, m – 22S/(22S + 22R) 17α,21β–C_{32} homohopane, n – 17α–C_{27} trisnorhopane/(17α–C_{27} trisnorhopane+18α–C_{27} trisnorneohopane (Ts/(Ts + Tm)), o – %$Rc_{(MPI\ 1)}$ (Radke and Welte, 1983), p – DBT/P (Hughes et al., 1995).

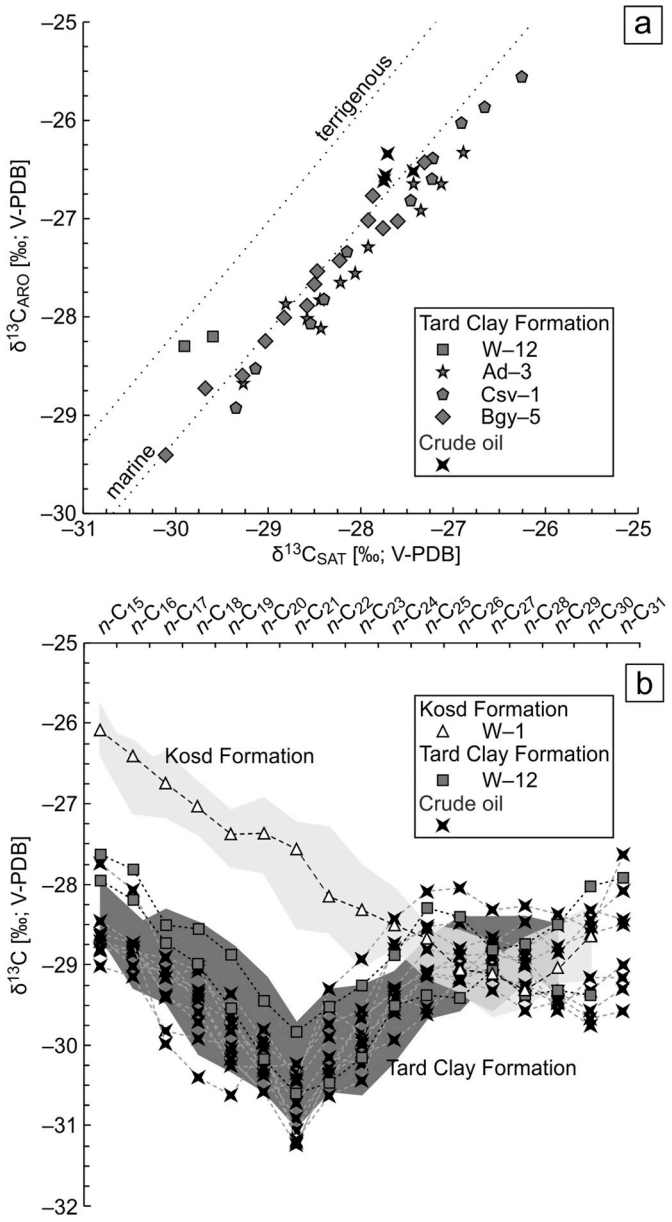

Fig. 10. Stable carbon isotope composition of the a) saturated and aromatic hydrocarbon fraction of the Tard Clay and crude oil samples. The $\delta^{13}C$ values of the Tard Clay from Ad–3, Csv–1 and Bgy–5 wells are taken from Bechtel et al. (2012). The marine and terrigenous lines are based on Sofer (1984). (b) Compound-specific isotope of *n*-alkanes in the studied samples. The grey shaded areas represent $\delta^{13}C$ values of the Tard Clay (Bechtel et al., 2012) and Kosd Formation (Körmös et al., 2020). Mean values of four samples are presented for Kosd Formation from W–1 well.

et al., 2006; Meyers, 1997), and species, photosynthesizing according to the C3 pathway, were noticed before (e.g. Ficken et al., 1998; Mortillaro et al., 2016). The high-molecular weight *n*-alkanes (*n*-$C_{27–31}$) were derived from plant-waxes (Eglinton and Hamilton, 1967) and reached a maximum of 35% of the total *n*-alkanes in sample W–10o (Table 2). The $\delta^{13}C$-values are comparable with the typical carbon isotope values of C3 plants (e.g. Meyers, 1997). Terrestrial plants employ atmospheric CO_2 during photosynthesis (Lamb et al., 2006; Meyers, 1997) but the biosynthesis and maturation-induced fractionations of carbon isotopes vary among plant types (Diefendorf et al., 2011, 2015; Lockheart et al., 1997) and are comparable with the observed values.

The V-shape character of the compound-specific stable carbon isotope in the range of short- and mid-chain *n*-alkanes (Fig. 10b; Table 4)

Table 4
Compound-specific stable carbon isotope of investigated oil samples.

ID	*n*-C_{15}	*n*-C_{16}	*n*-C_{17}	*n*-C_{18}	*n*-C_{19}	*n*-C_{20}	*n*-C_{21}	*n*-C_{22}	*n*-C_{23}	*n*-C_{24}	*n*-C_{25}	*n*-C_{26}	*n*-C_{27}	*n*-C_{28}	*n*-C_{29}	*n*-C_{30}	*n*-C_{31}
#									[‰; V-PDB]								
W–1o	−28.8	−28.9	−28.9	−29.1	−29.6	−30.3	−30.9	−30.4	−29.7	−29.3	−29.1	−29.2	−28.8	−29.0	−29.6	−29.2	−29.2
W–2o	−28.7	−29.0	−29.1	−29.3	−29.4	−30.0	−31.2	−30.4	−30.0	−29.4	−29.5	−29.2	−28.9	−28.9	−29.4	−29.7	−29.6
W–3o	n.d.	−28.9	−29.2	−29.0	−29.8	−30.4	−31.1	−30.3	−29.7	−29.4	−29.1	−29.0	−29.1	−29.3	−29.5	−29.8	n.d.
W–5o	−28.6	−28.7	−29.4	−29.6	−30.3	−30.3	−30.2	−29.7	−29.6	−28.8	−28.5	−28.5	−28.7	−28.5	−28.9	−28.4	−28.1
W–6o	−28.8	−28.8	−29.4	−29.7	−30.2	−30.6	−30.5	−29.9	−29.9	−28.7	−28.6	−28.8	−28.7	−28.8	−28.5	−28.3	−28.4
W–8o	−27.7	−28.1	−28.9	−29.4	−30.1	−29.8	−30.4	−29.3	−28.9	−28.4	−28.1	−28.1	−28.3	−28.3	−28.4	−28.6	−27.6
W–10o	−29.0	−29.2	−29.8	−29.9	−30.0	−30.0	−30.4	−29.5	−29.9	−29.6	−29.1	−29.2	−29.3	−29.6	−29.5	−29.3	−29.0
W–11o	−28.7	−28.8	−29.2	−29.4	−30.2	−30.6	−31.2	−30.4	−30.1	−29.9	−29.6	−29.2	−29.0	−29.4	−29.3	−29.6	−29.3
W–12o	n.d.	−28.8	−29.1	−29.4	−29.7	−30.2	−30.7	−30.1	−30.2	−29.6	−29.1	−28.9	−29.1	−29.3	−29.4	n.d.	n.d.
W–13o	−28.5	−28.7	−30.0	−30.4	−30.6	−30.0	−31.2	−30.6	−30.4	−29.3	−28.8	−28.9	−28.9	−29.0	−28.8	−28.6	−28.5

Table 5
Source- and maturity-related biomarker and non-biomarker indices of the selected source rock samples.

Fms	Well	Depth [m; MD]	a [%]	b [%]	c	d	e	f	g	h	i	j	k	l	m	n	o	p	q	r	s	t	u	v	w [%]	x
Kosd Formation	W–1	2599.9	14	23	63	0.37	0.06	0.09	0.50	0.67	28.80	10.59	1.18	1.57	0.34	0.01	0.28	0.35	0.38	0.66	0.06	0.06	0.57	0.29	0.71	0.84
		2600.9	17	17	66	0.26	0.07	0.08	0.45	0.67	10.66	4.65	0.99	1.13	0.33	0.04	0.78	0.56	0.45	0.75	0.06	0.11	0.59	0.27	0.73	1.00
		2601.2	21	27	52	0.52	0.07	0.12	0.42	0.66	2.70	1.53	1.41	1.19	0.34	0.33	0.96	0.51	0.67	0.59	0.05	0.15	0.63	0.20	0.72	1.01
		2602.0	18	20	62	0.32	0.09	0.11	0.49	0.69	8.26	4.13	1.03	0.75	0.39	0.02	0.62	0.41	0.35	0.65	0.06	0.06	0.57	0.44	0.72	0.94
Tard Clay Formation	W–12	2250.0	24	44	32	1.39	0.04	0.30	0.52	0.58	0.23	0.42	0.63	0.71	1.07	0.02	0.12	0.38	0.38	0.89	0.13	0.26	0.59	0.48	0.72	0.18
		2260.0	32	36	33	1.08	0.06	0.42	0.54	0.47	0.47	0.80	0.62	0.63	1.01	0.02	0.10	0.42	0.29	0.77	0.10	0.15	0.57	0.49	0.74	0.23
		2294.6	43	16	40	0.40	0.14	0.32	0.52	0.58	0.44	0.74	0.73	0.38	0.69	0.01	0.08	0.40	0.21	0.41	0.05	0.12	0.55	0.58	0.74	0.12
		2298.1	32	29	39	0.74	0.16	0.16	0.50	0.63	0.73	0.69	0.96	0.58	1.01	0.05	0.23	0.44	0.25	0.75	0.08	0.16	0.57	0.53	0.76	0.11

Fms – formations, a – C_{27} steranes/Σ regular steranes, b – C_{28} steranes/Σ regular steranes, c – C_{29} steranes/Σ regular steranes, d – C_{28}/C_{29} steranes, e – C_{21-22}/C_{27-29} steranes, f – C_{27} diaS/(diaS + regS), g – 20S/(20S + 20R) ααα C_{29} sterane, h – αββ/(αββ+ααα) C_{29} sterane, i – C_{19}/C_{23}TT, j – C_{20}/C_{23}TT, k – C_{21}/C_{23}TT, l – C_{24}/C_{23}TT, m – C_{26}/C_{25}TT, n – C_{23} TT/H, o – Ol/(Ol + H), p – NH/H, q – C_{31}(R)/H, r – C_{35}(S)/C_{34}(S), s – C_{35}/C_{31-35}, t – steranes/hopanes, u – 22S/(22S + 22R) 17α,21β–C_{32} homohopane, v – Ts/(Ts + Tm), w – $\%Rc_{(MPI\ 1)}$ (Radke and Welte, 1983), x – DBT/P (Hughes et al., 1995).

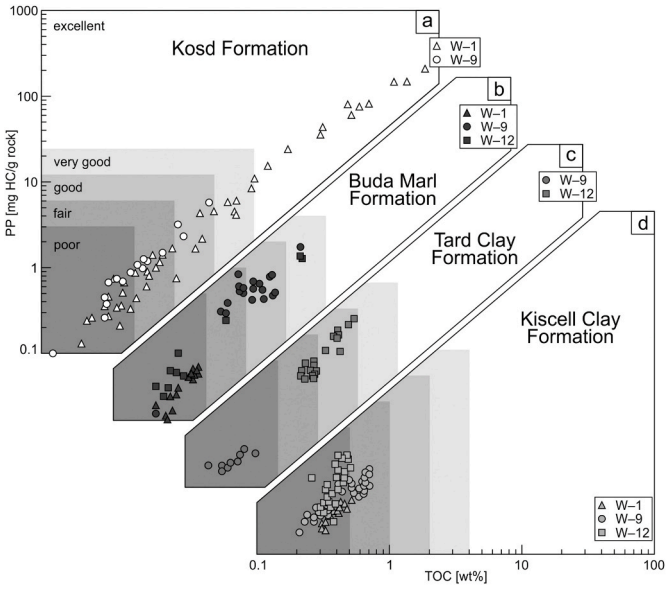

Fig. 11. Assessment of the hydrocarbon generation potential (modified after Peters and Cassa 1994) for the a) Kosd Formation, b) Buda Marl Formation, c) Tard Clay Formation and d) Kiscell Clay Formation.

could not be explained based on the mechanism of the carbon assimilation by primary producers. Bacteria may have an impact on the isotope composition as they produce short- and mid-chain *n*-alkanoic acids, *n*-alkanols and *n*-alkanes (e.g. Pearson et al., 2007), which were noticed to be enriched in ^{12}C with increasing chain length (e.g. Shah et al., 2013). Nevertheless, extensive heterotrophic consumption of organic matter is not expected because of the negligible fractionation of carbon isotopes between bacterial heterotrophs and source organic carbon (Blair et al., 1985). On the contrary, the metabolism of chemoautotroph bacteria may yield ^{13}C depleted compounds (Shah et al., 2013; Wakeham et al., 2007) and is probably responsible for the V-shape pattern of *n*-alkane carbon isotope. The stable carbon isotope composition and distribution of the *n*-alkanes (Figs. 5a and 10b; Tables 2 and 4), and the ratio of the isoprenoids to *n*-alkanes (Fig. 6) suggest organic matter from mixed marine/lacustrine and terrigenous, bacterial sources.

The distribution of regular steranes indicate a slight dominance of C_{29} and C_{28} homologues over C_{27}, but the minimum percentage of the C_{27} homologue is still 23% (e.g. W–11o; Figs. 7a and 8; Table 2). Algae were identified as the primary producer of the C_{27} sterols (Volkman, 1986). Moreover, microalgae could contain a substantial amount of 24–ethylcholesterol (Volkman et al., 1999). Furthermore, the 24–*n*–propylcholestane confirms the contribution of marine algae (Chrysophyte; Moldowan et al., 1990) to organic matter. The C_{29} sterols are typically assigned to terrestrial origin (e.g. land plants; Volkman, 1986). The C_{28} sterols are derived from diverse precursors (Grantham and Wakefield, 1988; Peters et al., 1989, 2000), but the high contribution of C_{28} steranes (Fig. 8) and high ratio of C_{28}/C_{29} steranes (Table 2) argue for an origin related to phytoplankton (e.g. diatoms, coccolithophores, dinoflagellates; Grantham and Wakefield, 1988). That is also supported by the presence of C_{30}–methylsteranes derived from 4α–methylsterols, indicative of the presence of dinoflagellates (Wolff et al., 1986). The relative abundances of the regular steroids argue for an open and shallow marine paleoenvironment with biomass that includes marine or brackish phytoplankton assemblages, living in the photic zone of the water column, and the contribution of terrestrial organic matter (e.g. vascular plants; Fig. 8).

The ratios of C_{19}/C_{23}TT and C_{20}/C_{23}TT could reflect the relative distribution of terrigenous and marine organic matter (e.g. Tao et al., 2015; Xiao et al., 2019). The C_{19}TT and C_{20}TT occur in higher concentration in terrestrial oils, whereas the C_{23}TT is frequently detected as the

dominant TT in marine oils (Aquino Neto et al., 1983; Ekweozor and Strausz, 1983; Peters and Moldowan, 1993). The high abundance of C_{23}TT and low ratios of C_{19}/C_{23}TT and C_{20}/C_{23}TT suggest the dominance of marine organic matter in the precursor biomass of crude oils (Fig. 7b; Table 3). Nevertheless, the occurrence of C_{24}TeT (e.g. 10β(H)–des–A–oleanane and 10β(H)–des–A–lupane; Woodhouse et al., 1992; Xiao et al., 2018) and 18α(H)–oleanane (Ekweozor et al., 1979) indicate the contribution of vascular plants (e.g. angiosperms) to the organic matter (Fig. 7b).

Beside the *n*-alkane distribution and composition of steroids and terpenoids, the stable carbon isotope composition of hydrocarbon fractions (Fig. 10a; Table 3) point to the dominance of marine biological precursors (Sofer, 1984).

The identified hopane derivatives (Fig. 7b) could originate from bacteriohopanepolyols (Ourisson et al., 1979; Rohmer, 1993), identified in bacteria and some cryptogames (e.g. moss, ferns). Beside the compound-specific carbon isotope, the low sterane to hopane ratios (Table 3) also suggest a microbially altered organic matter (Tissot and Welte, 1984) and can be assigned to a special bacteria-influenced depositional environment (Mackenzie, 1984). The plot of DBT/P *vs.* Pr/Ph points to a marine/lacustrine environment (Fig. 9). The presence of diasteranes (Fig. 7a) and ratios of C_{27} diasteranes and C_{27} regular steranes (C_{27} diaS/(diaS + regS); Table 2) emphasise the extent of the clay catalytic effect during diagenesis (Sieskind et al., 1979). Both, the ratios of C_{26}/C_{25}TT *vs.* C_{31}(R)/H and NH/H *vs.* C_{35}(S)/C_{34}(S) suggest that a marine shale is the most probable source rock of the crude oils studied (Fig. 12a and b; Peters et al., 2005).

The Pr/Ph ratio is a potential indicator of redox conditions and the determined ratios between one and three (avg. 1.88; Table 2) were proposed to indicate dysoxic conditions during sedimentation (Didyk et al., 1978). However, the Pr/Ph ratio could be influenced by thermal maturation (Radke et al., 1980a; Tissot and Welte 1984) and differences of the precursor organic matter (Blumer et al., 1963; Goossens et al., 1984; Volkman and Maxwell 1986; ten Haven et al., 1987; Rowland, 1990). Dysoxic conditions are also supported by the cross plot of phytane/*n*-C_{18} *vs.* pristane/*n*-C_{17} (Fig. 6) and the occurrence of des-A-triterpenes (Connan and Cassou, 1980; Jacob et al., 2007, and references therein).

The C_{35} hopanes are present in subordinate amounts than any other homohopanes in all investigated samples, and the homohopane index remains below 0.12 (Fig. 7b; Table 3). Similarly, the NH/H ratio does not reach 0.5, except in the most mature W–13o oil (Table 3). High concentrations of C_{35} hopanes and C_{29} 17α–norhopanes were interpreted as indicators of strongly reducing conditions during deposition, but maturity also affects the ratios (Peters and Moldowan, 1991).

The DBT/P ratios are low and reach a maximum of 1.27 only in the early mature oil W–11o (Table 3), indicating generally low but varying amounts of free H_2S near the sediment-water interface during source rock deposition. Low sterane to hopane ratios and the V-shape pattern of *n*-alkane isotope evidence strong bacterial activity (Table 3). Accordingly, the bacterial sulphate reduction probably transformed the available reactive iron, incorporated onto clay minerals and the sulphide phases into pyrite framboids (Casagrande, 1987; Maclean et al., 2008; Morad, 1998; Sweeney and Kaplan, 1973), indicating, at least, locally reducing conditions.

The C_{21} pregnane and homopregnane are present in high abundance in most oils (Fig. 7a; Table 2). ten Haven et al. (1986) demonstrated that pregnane is often enhanced in hypersaline environments, but pregnanes are also known to be enriched in biodegraded oils (Peters et al., 2005). In the case of the studied oils, *n*-alkane distributions (Fig. 5a) and low proportions of isoprenoids relative to *n*-alkanes (Fig. 6) do not indicate biodegradation. Nevertheless, considering the low gammacerane peaks (Fig. 8b), hypersaline conditions during source rock deposition are unlikely.

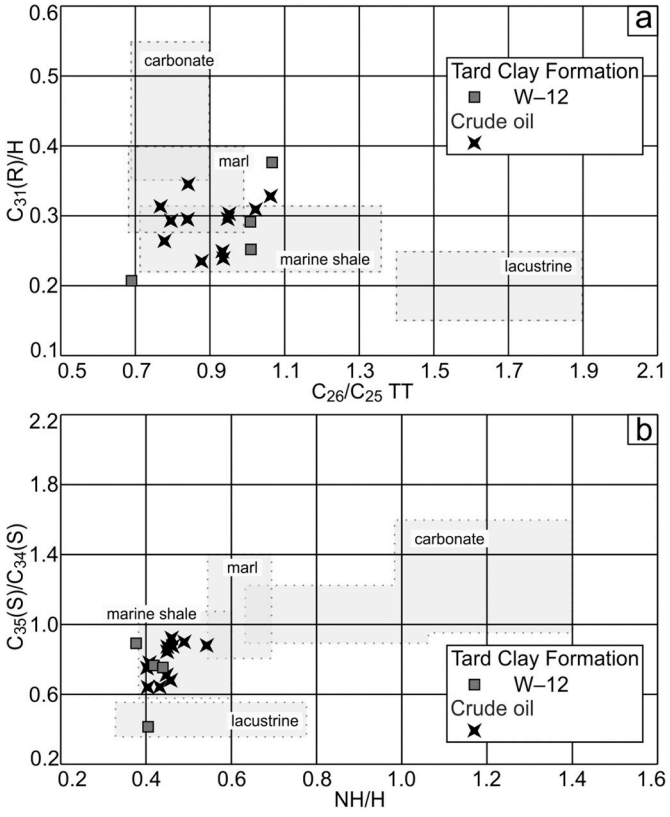

Fig. 12. The appraisal of the depositional environment based on biomarker and non-biomarker ratios. Cross plots of the a) C_{26}/C_{25} tricyclic terpanes *vs.* C_{31}(R)/H hopanes (after Peters et al., 2005), b) NH/H hopanes *vs.* C_{35}(S)/C_{34}(S) hopanes (after Peters et al., 2005).

5.3. Oil-to-source rock correlation

The occurrence of 18α(H)–oleanane (Fig. 7b) and high ratios of C_{28}/C_{29} steranes (Table 2) in the crude oils suggest an Upper Cretaceous or younger age of the potential source rocks. Furthermore, the source-related biomarker indicators suggest marine/lacustrine shales as the most potential source rocks of the oils.

These criteria comply for all investigated source rock formations, but the Kiscell Clay Formation is not considered further because of its poor petroleum potential. Biomarker data are available for the Tard Clay Formation from different locations in the Hungarian Palaeogene Basin (Bechtel et al., 2012). This study includes five additional Tard Clay samples from well W–12. The Kosd Formation in well W–1 was studied recently by Körmös et al. (2020). Table 5 lists the maturity- and source-related biomarker parameters for the Kosd and Tard Clay formation samples and used for oil-to-source rock correlation.

5.3.1. Thermal maturity

In the deep borehole W–12, the organic matter is marginally mature below 2230 m depth as indicated by Tmax values. The same maturity was recorded in well W–9 below 2500 m, and in well W–1 at 2100 m (Appendix A, B and C). Tmax values exceeding 435 °C (up to 451 °C) suggest oil window maturity (Appendix A, B and C; Bordenave et al., 1993). In contrast, in the shallow boreholes Ad–3, Csv–1 and Bgy–5, the organic matter is immature (Bechtel et al., 2012). Badics and Vető (2012) and Körmös et al. (2020) presented variations in the thermal maturity of the Tard Clay and Kosd Formation across the Hungarian Palaeogene Basin. The vast extension and great thickness of the investigated sediments point to local and large-scale differences in maturity within the studied formations.

Sterane and hopane isomerisation ratios for rock extracts and oils were calculated for further thermal maturity assessment. The ratios of

17α,21β(H)–C_{32} stereoisomers, 22S/(22S + 22R) are in equilibrium (Tables 3 and 5; Mackenzie et al., 1982; Seifert and Moldowan, 1980), suggesting that oil generation in the early phase (Peters et al., 2005) was reached in case of the Tard Clay (avg. 0.57) and Kosd (avg. 0.59) formations in the deep wells and by the crude oils (avg. 0.58). The S/(S + R) isomerisation ratios of the 5α,14α,17α(H)–C_{29} steranes (Tables 2 and 5) are close to the equilibrium value (0.55; Mackenzie and Maxwell, 1981; Seifert and Moldowan, 1986). Also, the ratios of the ββ/(ββ+αα) isomers of the C_{29} steranes equilibrate in the crude oils (avg. 0.71; Table 2), whereas, source rock samples are characterised by lower values (avg. 0.67 and 0.57, respectively; Table 5; Seifert and Moldowan, 1986). The range of both sterane isomerisation ratios indicates mature samples in the peak oil window range (Peters et al., 2005).

CPI values of crude oils close to one (Table 2) also agree with this maturity assessment. Additionally, the ratios of 17α–trisnorhopane and 18α–trisnorneohopane (Ts/(Ts + Tm); Tables 3 and 5; Seifert and Moldowan, 1978) support the previous assumption. Even though the Ts/(Ts + Tm) ratios are strongly affected by differences in source facies (Seifert and Moldowan, 1978), the values of Tard Clay (0.48–0.58; Table 5) and crude oils are in the same range (0.46–0.62; Table 3).

Thermal maturity controls the distributions of methyl-homologues of phenanthrene in the range of 0.6–1.7% vitrinite reflectance (Radke et al., 1982b). The methylphenanthrene index (MPI 1) is a well-established non-biomarker maturity parameter (Radke et al., 1982a, 1982b) and was used to determine the vitrinite reflectance ($Rc_{(MPI\ 1)}$; Radke and Welte, 1983). The calculated $Rc_{(MPI\ 1)}$ values indicate peak oil window maturity for crude oils (0.76–0.96% $Rc_{(MPI\ 1)}$; Table 3) and slightly lower maturity for source rocks (0.71–0.76% $Rc_{(MPI\ 1)}$; Table 5). The MPI 1 was calibrated using type III kerogen (e.g. coal); thus, the calculated vitrinite reflectance values could be biased by the mixture of the marine and terrigenous organic matter.

Considering the variable thickness and great lateral extent of the Tard Clay and Kosd formations (e.g. Badics and Vető, 2012; Körmös et al., 2020), local- and large-scale variations in thermal maturity were expected. Such differences are reflected by the immature character of the Tard Clay in wells Ad–3, Csv–1 and Bgy–5 (Bechtel et al., 2012), contrasting the results of samples from boreholes W–9 and W–12, indicating oil window maturity (Fig. 4c). The determined thermal maturity parameters are comparable between the source rock extracts from the deep boreholes (W–1 and W–12) and crude oils. However, based on phytane/*n*-C_{18} *vs.* pristane/*n*-C_{17} ratios (Fig. 6) and $Rc_{(MPI\ 1)}$% (Tables 3 and 5) the crude oils are thermally more mature, especially in samples W–12o and W–13o (Table 2), which originate from carbonate reservoirs in the eastern part of the research area.

The sterane isomerisation ratios (20S/(20S + 20R); Table 2) and $Rc_{(MPI\ 1)}$% values (Table 3) show an increasing depth trend in wells W–1 to W–7 (W–1o to W–7o; Fig. 1; Table 1) in the central part of the study area, which could indicate that (i) oils (W–8o to W–12o; Tables 2 and 3) experienced vertical migration, and (ii) source rocks maturity is greater in areas of W–13 well (W–13o; Table 3).

5.3.2. *Biomarker and non-biomarker indices*

In the shallow boreholes, the stable carbon isotope composition in the hydrocarbon fraction of the Tard Clay follows and stretches along the marine line, as proposed by Sofer (1984; Fig. 10a). In the deep well W–12, the $\delta^{13}C$ values suggest a greater contribution of terrestrial organic matter (e.g. land plants as evidenced by the OI/(OI + H); Table 5), which could be the result of the proximity of the paleo-shoreface. In contrast, the $\delta^{13}C$ values of the oils point to a dominant marine organic matter input (Fig. 10a).

Compound-specific stable carbon isotope analysis of *n*-alkanes is an important approach in correlation studies (e.g. Bjorøy et al., 1994; Cheng et al., 2015; Pedentchouk and Turich, 2017). Isotope patterns of *n*-alkanes are different between oil samples and extracts from Eocene rocks; however, there is an apparent fit between oil and Tard Clay core samples, with both sample sets showing a distinct V-shape pattern (Fig. 10b), which also indicates that the mixing of different oils can be ruled out in the present study. The *n*-alkanes in crude oils are slightly depleted in ^{13}C, which could be an effect of the thermal maturation (e.g. Bjorøy et al., 1992; Clayton, 1991; Rooney et al., 1998; Schoell, 1984). The variations in the $\delta^{13}C$ values are within 2‰, indicating a positive correlation between the sample sets (Sofer, 1984) and the stable carbon isotope composition of individual biological markers allows the identification of specific sources (Hayes et al., 1987). Bechtel et al. (2013), Mayer et al. (2018) and Sachsenhofer et al. (2019) studied Lower Oligocene source rock intervals in the Alpine Foreland Basin, western Black Sea, and along the Carpathians, and observed a very specific V-shaped stable carbon isotope pattern in organic matter rich sediments deposited during nannoplankton zones NP 21, NP 22 and the lowermost part of NP 23, coeval with the Buda Marl and Tard Clay formations in the Hungarian Palaeogene Basin (Fig. 2).

Despite the positive correlation, confirmed by compound-specific stable carbon isotope, the source-related biomarker parameters indicate subtle differences between the crude oils and Tard Clay. The most obvious differences concern higher DBT/P values and higher sterane to hopane ratios in crude oils compared to extracts from the Tard Clay in the deep well W–12 (Tables 3 and 5). Higher DBT/P values may reflect variations in the amount of free H_2S as a result of varying iron availability, whereas higher sterane to hopane ratios and the V-shape pattern of the *n*-alkane isotope may express (chemoautotroph) bacterial activity due to water column stratification, as already detected within the Oligocene Tard Clay and Schöneck formations by Bechtel et al. (2012) and Schulz et al. (2002), respectively. Water column stratification is suggested by high pregnanes concentrations, sulphur aromatic compounds and the occurrence of (low amounts of) gammacerane (Figs. 5b and 7). Bechtel et al. (2012) and Ozsvárt et al. (2016) revealed different depositional environments, characterised by varying salinity and the occurrence of bottom water anoxia during the accumulation of the Tard Clay. These conditions are favourable for both the activity of sulphate reducing bacteria and the incorporation of sulphur phases into organic compounds, resulting in variable content of sulphur aromatic compounds in crude oils. Thus, the differences in molecular composition between the crude oils and Tard Clay extracts are likely caused by variations in the source facies described by Bechtel et al. (2012) and Ozsvárt et al. (2016).

The Tard Clay is the most apparent source for the accumulated oils. However, based on the V-shape compound-specific carbon isotope pattern (Fig. 10b), which suggest deposition of the source rock during NP 21 to NP 23 (Sachsenhofer et al., 2019), a contribution from the Buda Marl (NP 19–21; Fig. 2) cannot be excluded. It is reasonable to assume that during the Eocene-Oligocene transition the continuous deepening of the Hungarian Palaeogene Basin (Nagymarosy et al., 1986) resulted in conditions favourable for organic matter enrichment. Within this context, it is important to note that Buda Marls in well W–9 contain a maximum of 2.7 wt% TOC (Fig. 3) and are characterised by a fair petroleum potential (Fig. 11b). Therefore, detailed organic geochemical studies of the Buda Marls are highly recommended.

6. Conclusion

The detailed organic geochemical investigation of the Upper Eocene and Lower Oligocene source rocks and accumulated oils in the Hungarian Palaeogene Basin led to the following conclusions.

The sediments of the Kosd, Buda Marl and Tard Clay formations are identified as hydrocarbon generating source rocks. In contrast, the involved rocks of the Kiscell Clay Formation are interpreted as non-source rocks. The spatial distribution and Rock-Eval characteristics of the former formations indicate diverse petroleum potential along the study area.

The molecular composition of accumulated crude oils determines the Tard Clay as the most probable source rock. Minor differences in source-related biomarker parameters are assumed to be caused by vertical and

lateral variations in the source facies.

Considering the maturity parameters and the common V-shape pattern in the compound-specific carbon isotope profile of *n*-alkanes in sediment extracts, deposited during NP 21 to NP 23, a contributing source from the Buda Marl is assumable. Therefore, detailed organic geochemical studies of the Buda Marls are highly recommended to explore the significance of these findings.

CRediT author statement

Sándor Körmös: Conceptualization, Investigation, Writing - Original Draft, Visualization, Writing - Review & Editing, **Reinhard F. Sachsenhofer:** Writing - Review & Editing, Supervision, **Achim Bechtel:** Investigation, Writing - Review & Editing, **Balázs Géza Radovics:** Writing - Review & Editing, Formal analysis, **Katalin Milota:** Formal analysis, **Félix Schubert:** Writing - Review & Editing, Supervision.

Declaration of competing interest

The authors declare that they have no known competing financial interests or personal relationships that could have appeared to influence the work reported in this paper.

Acknowledgement

The authors thankfully acknowledge MOL Plc for providing the samples and permitting the submission of the manuscript. We thank JMPG editor-in-chief Dr. Qinhong Hu, section editor Dr. Hui Tian and two anonymous reviewers for their constructive comments. The study was achieved during the term of the Ernst Mach and Campus Mundi scholarship periods of SK, funded by 'Stiftung Aktion Österreich-Ungarn' (ICM-2018-12611) and Tempus Public Foundation (CM-SMR-421662-2020). This work was sponsored by the National Research, Development and Innovation Fund, Cooperative Doctoral Programme (975153) Ministry for Innovation and Technology, Hungary, and the University of Szeged Open Access Fund (5057).

Appendices

Appendix A

Bulk geochemical parameters of investigated samples from well W–1.

Fms	ID	Depth	TOC	S1	S2	HI	PP	PI	Tmax
	#	[m; MD]	[wt%]	[mg HC/g rock]		[mg HC/g TOC]	[mg HC/g rock]		[°C]
Kiscell Clay Formation	1	2100.0	0.52	0.0	0.4	81	0.43	0.02	434
	2	2120.0	0.48	0.0	0.3	69	0.34	0.03	434
	3	2130.0	0.46	0.0	0.4	83	0.39	0.03	435
	4	2140.0	0.42	0.0	0.3	79	0.34	0.03	438
	5	2150.0	0.38	0.0	0.3	82	0.32	0.03	435
	6	2160.0	0.43	0.0	0.4	93	0.41	0.02	438
	7	2170.0	0.36	0.0	0.3	75	0.28	0.04	437
	8	2180.0	0.42	0.0	0.3	69	0.30	0.03	435
	9	2190.0	0.16	0.0	0.1	56	0.09	0.00	434
	10	2200.0	0.33	0.0	0.2	55	0.19	0.05	434
	11	2210.0	0.31	0.0	0.2	71	0.23	0.04	435
	12	2220.0	0.31	0.0	0.2	61	0.20	0.05	433
	13	2230.0	0.33	0.0	0.2	70	0.23	0.00	435
	14	2240.0	0.41	0.0	0.3	73	0.31	0.03	439
Buda Marl Formation	15	2250.0	0.41	0.0	0.3	80	0.34	0.03	437
	16	2260.0	0.44	0.0	0.3	77	0.35	0.03	442
	17	2270.0	0.44	0.0	0.4	91	0.42	0.05	439
	18	2280.0	0.37	0.0	0.3	84	0.32	0.03	435
	19	2290.0	0.38	0.0	0.3	82	0.32	0.03	441
	20	2300.0	0.39	0.0	0.3	82	0.33	0.03	438
	21	2310.0	0.40	0.0	0.4	98	0.40	0.03	439
	22	2320.0	0.40	0.0	0.3	75	0.30	0.00	439
	23	2330.0	0.31	0.0	0.2	74	0.24	0.04	438
	24	2340.0	0.27	0.0	0.2	70	0.19	0.00	438
	25	2350.0	0.25	0.0	0.1	44	0.11	0.00	439
	26	2360.0	0.30	0.0	0.2	63	0.20	0.05	438
	27	2370.0	0.21	0.0	0.2	71	0.15	0.00	442
	28	2380.0	0.17	0.0	0.1	35	0.06	0.00	444
	29	2390.0	0.26	0.0	0.1	38	0.10	0.00	443
	30	2400.0	0.28	0.0	0.1	46	0.13	0.00	442
	31	2410.0	0.23	0.0	0.1	35	0.08	0.00	439
Kosd Formation	32	2420.0	0.69	0.1	1.3	193	1.40	0.05	440
	33	2430.0	0.63	0.3	0.6	95	0.90	0.33	443
	34	2450.0	0.35	0.0	0.7	200	0.74	0.05	442
	35	2470.0	0.41	0.0	0.5	115	0.51	0.08	445
	36	2490.0	0.62	0.1	0.5	84	0.60	0.13	442
	37	2497.0	0.73	0.2	0.8	114	1.00	0.17	442
	38	2502.0	1.63	0.4	1.8	111	2.17	0.17	442
	39	2510.0	0.37	0.0	0.3	84	0.34	0.09	444
	40	2530.0	0.30	0.0	0.3	107	0.35	0.09	446
	41	2550.0	0.24	0.0	0.2	100	0.26	0.08	447
	42	2570.0	0.40	0.1	0.3	75	0.36	0.17	448
	43	2575.0	0.65	0.2	0.6	98	0.80	0.20	443
	44	2580.0	0.32	0.1	0.4	109	0.46	0.24	442

(*continued on next page*)

Appendix A (*continued*)

Fms	ID	Depth	TOC	S1	S2	HI	PP	PI	Tmax
	#	[m; MD]	[wt%]	[mg HC/g rock]		[mg HC/g TOC]	[mg HC/g rock]		[°C]
	45	2585.0	2.00	0.9	3.7	185	4.54	0.19	445
	46*	2590.0	29.55	10.0	71.9	243	81.83	0.12	441
	47*	2590.2	7.23	2.5	20.9	289	23.39	0.11	443
	48*	2594.4	0.39	0.1	0.1	36	0.21	0.33	439
	49*	2594.6	12.72	3.8	31.9	251	35.65	0.11	441
	50*	2594.9	1.45	0.7	1.0	68	1.66	0.40	439
	51	2595.0	13.25	5.1	38.7	292	43.71	0.12	441
	52*	2596.8	0.51	0.5	0.3	66	0.87	0.61	446
	53*	2599.0	1.04	0.4	0.4	39	0.75	0.47	431
	54*	2599.9	78.39	23.4	186.3	238	209.64	0.11	443
	55*	2600.0	2.94	1.1	3.0	103	4.14	0.27	443
	56	2600.0	20.46	9.2	71.2	348	80.42	0.11	447
	57*	2600.6	2.89	1.5	2.9	101	4.42	0.34	445
	58*	2600.9	45.70	14.6	133.1	291	147.61	0.10	441
	59*	2601.0	3.84	1.8	6.6	171	8.40	0.22	448
	60*	2601.2	25.04	9.3	66.1	264	75.45	0.12	440
	61*	2601.4	2.96	1.1	4.9	165	6.05	0.19	446
	62*	2602.0	21.82	6.6	53.8	247	60.37	0.11	438
	63	2602.0	2.54	1.1	4.8	188	5.82	0.18	450
	64*	2602.4	0.97	0.9	0.8	82	1.67	0.52	444
	65*	2604.1	0.78	0.4	0.7	92	1.16	0.38	443
	66*	2604.9	57.17	17.2	130.8	229	147.97	0.12	444
	67*	2605.0	0.82	0.5	0.9	107	1.41	0.38	444
	68	2610.0	5.10	2.0	13.4	263	15.39	0.13	448
	69	2630.0	1.57	1.1	3.2	204	4.31	0.26	448
	70	2650.0	4.05	1.9	9.1	224	10.94	0.17	442
	71	2670.0	0.42	0.1	0.6	138	0.67	0.13	444
	72	2695.0	0.22	0.1	0.2	86	0.24	0.21	444
	73	2710.0	0.20	0.0	0.1	55	0.13	0.15	447
	74	2730.0	0.32	0.1	0.2	69	0.27	0.19	447
	75	2750.0	0.47	0.0	0.3	66	0.33	0.06	451
	76	2770.0	0.52	0.0	0.4	77	0.44	0.09	442
	77	2790.0	0.10	0.0	0.1	50	0.05	0.00	443

Fms – formations, TOC – total organic carbon content, S1 – free hydrocarbons, S2 – hydrocarbons generated during Rock-Eval pyrolysis, HI – hydrogen index, PP – petroleum potential, PI – production index, Tmax – temperature of maximum hydrocarbon generation, MD – measured depth, * – drill core sample.

Appendix B

Bulk geochemical parameters of investigated samples from well W–9.

Fms	ID	Depth	TOC	S1	S2	HI	PP	PI	Tmax
	#	[m, MD]	[wt%]	[mg HC/g rock]		[mg HC/g TOC]	[mg HC/g rock]		[°C]
Kiscell Clay Formation	1	1800	0.54	0.1	0.5	87	0.52	0.10	427
	2	1820	0.59	0.0	0.4	73	0.47	0.09	428
	3	1840	0.59	0.0	0.6	93	0.59	0.07	428
	4	1860	0.64	0.0	0.5	84	0.57	0.05	428
	5	1880	0.64	0.0	0.5	75	0.51	0.06	430
	6	1900	0.65	0.0	0.5	77	0.54	0.07	429
	7	1920	0.71	0.1	0.6	82	0.63	0.08	432
	8	1940	0.71	0.1	0.6	83	0.64	0.08	428
	9	1960	0.71	0.1	0.8	115	0.88	0.07	430
	10	1980	0.67	0.1	0.6	90	0.67	0.10	429
	11	2000	0.66	0.1	0.6	86	0.64	0.11	428
	12	2020	0.66	0.0	0.6	94	0.65	0.05	431
	13	2040	0.69	0.1	0.8	122	0.90	0.07	434
	14	2060	0.65	0.1	0.7	111	0.78	0.08	432
	15	2080	0.65	0.1	0.7	105	0.74	0.08	431
	16	2100	0.71	0.1	0.9	121	0.94	0.09	432
	17	2120	0.65	0.1	0.7	106	0.74	0.07	433
	18	2140	0.62	0.1	0.6	100	0.69	0.10	433
	19	2160	0.69	0.1	0.8	120	0.91	0.09	432
	20	2180	0.66	0.1	0.8	123	0.88	0.08	433
	21	2200	0.50	0.1	0.7	130	0.72	0.10	432
	22	2220	0.52	0.1	0.5	102	0.59	0.10	429
	23	2240	0.44	0.1	0.5	109	0.54	0.11	431
	24	2260	0.52	0.1	0.6	117	0.67	0.09	432
	25	2300	0.35	0.1	0.2	69	0.29	0.17	433
	26	2320	0.35	0.0	0.3	83	0.32	0.09	431
	27	2340	0.41	0.1	0.6	144	0.64	0.08	431
	28	2360	0.33	0.1	0.3	88	0.37	0.22	433
	29	2380	0.28	0.0	0.3	111	0.35	0.11	433
	30	2400	0.24	0.0	0.3	104	0.29	0.14	429

(*continued on next page*)

Appendix B (*continued*)

Fms	ID	Depth	TOC	S1	S2	HI	PP	PI	Tmax
	#	[m, MD]	[wt%]	[mg HC/g rock]		[mg HC/g TOC]	[mg HC/g rock]		[°C]
	31	2420	0.27	0.0	0.2	81	0.24	0.08	432
	32	2430	0.30	0.0	0.3	90	0.29	0.07	434
	33	2440	0.29	0.0	0.3	97	0.30	0.07	434
	34	2460	0.23	0.0	0.2	91	0.24	0.13	432
	35	2480	0.21	0.0	0.2	76	0.18	0.11	435
	36	2490	0.27	0.0	0.2	89	0.27	0.11	434
Tard Clay Formation	37	2500	0.28	0.0	0.3	89	0.28	0.11	434
	38	2510	0.34	0.0	0.2	65	0.25	0.12	435
	39	2520	0.26	0.0	0.2	77	0.24	0.17	437
	40	2530	0.25	0.0	0.2	76	0.20	0.05	435
	41	2540	0.22	0.0	0.2	73	0.19	0.16	437
	42	2550	0.21	0.1	0.1	57	0.17	0.29	437
	43	2560	0.15	0.1	0.1	87	0.18	0.28	435
	44	2570	0.19	0.0	0.1	68	0.16	0.19	435
	45	2580	0.19	0.1	0.1	63	0.17	0.29	434
Buda Marl Formation	46	2600	0.21	0.0	0.1	52	0.12	0.08	437
	47	2610	1.66	0.4	2.6	159	3.07	0.14	433
	48	2620	1.37	0.3	2.3	168	2.61	0.12	432
	49	2630	1.34	0.6	2.8	205	3.33	0.17	437
	50	2640	1.27	0.7	3.2	255	3.94	0.18	438
	51	2650	0.96	0.8	2.7	282	3.50	0.23	437
	52	2660	0.90	0.5	2.7	300	3.21	0.16	440
	53	2670	0.89	0.8	2.9	325	3.67	0.21	440
	54	2680	0.88	2.5	2.6	293	5.08	0.49	437
	55	2690	0.71	0.4	1.4	200	1.78	0.20	441
	56	2700	0.96	0.5	2.5	264	3.05	0.17	439
	57	2710	1.08	0.7	2.7	254	3.42	0.20	440
	58	2720	1.52	0.9	3.9	256	4.74	0.18	437
	59	2730	1.55	0.9	4.0	256	4.86	0.18	437
	60	2740	0.65	0.3	1.6	242	1.86	0.16	441
	61	2750	1.12	0.6	2.0	175	2.55	0.23	439
	62	2760	1.14	1.4	2.8	247	4.17	0.32	441
	63	2770	1.61	0.8	2.1	133	2.89	0.26	438
	64	2780	2.59	5.3	5.3	203	10.55	0.50	435
	65	2790	0.73	0.7	1.6	223	2.34	0.30	442
Kosd Formation	66	2800	0.32	0.2	0.5	153	0.67	0.27	438
	67	2810	1.84	2.6	3.2	173	5.76	0.45	437
	68	2820	0.41	0.2	0.5	110	0.69	0.35	437
	69	2830	0.63	0.3	0.9	135	1.19	0.29	440
	70	2840	1.07	0.9	2.3	214	3.19	0.28	435
	71	2850	0.59	0.3	0.9	158	1.26	0.26	439
	72	2860	0.53	0.3	0.8	153	1.08	0.25	437
	73	2880	0.58	0.3	0.7	124	0.98	0.27	440
	74	2890	1.18	0.7	1.6	137	2.32	0.30	434
	75	2900	0.82	0.3	1.2	140	1.49	0.23	442
	76	2910	0.37	0.2	0.5	146	0.74	0.27	441
	77	2920	0.47	0.2	0.7	138	0.88	0.26	431
	78	2930	0.30	0.1	0.3	113	0.45	0.24	438
	79	2940	0.31	0.1	0.3	84	0.38	0.32	437
	80	2950	0.13	0.0	0.1	54	0.10	0.30	–
	81	2960	0.13	0.0	0.0	31	0.06	0.33	–
	82	2970	0.30	0.1	0.2	57	0.26	0.35	–

Fms – formations, TOC – total organic carbon content, S1 – free hydrocarbons, S2 – hydrocarbons generated during Rock-Eval pyrolysis, HI – hydrogen index, PP – petroleum potential, PI – production index, Tmax – temperature of maximum hydrocarbon generation, MD – measured depth.

Appendix C

Bulk geochemical parameters of investigated samples from well W–12.

Fms	ID	Depth	TOC	S1	S2	HI	PP	PI	Tmax
	#	[m; MD]	[wt%]	[mg HC/g rock]		[mg HC/g TOC]	[mg HC/g rock]		[°C]
Kiscell Clay Formation	1	1960.0	0.44	0.1	1.2	282	1.32	0.06	431
	2	1970.0	0.41	0.0	0.6	139	0.59	0.03	432
	3	1980.0	0.35	0.0	0.4	126	0.46	0.04	433
	4	1990.0	0.38	0.0	0.4	95	0.37	0.03	432
	5	2000.0	0.39	0.0	0.4	97	0.40	0.05	433
	6	2010.0	0.41	0.1	0.9	220	0.96	0.06	–
	7	2020.0	0.41	0.1	0.9	327	1.43	0.06	–
	8	2030.0	0.40	0.1	1.3	188	0.79	0.05	–
	9	2040.0	0.49	0.0	0.8	237	1.29	0.10	–
	10	2050.0	0.26	0.1	1.2	277	0.78	0.08	–
	11	2060.0	0.48	0.1	0.7	265	1.44	0.12	–

(*continued on next page*)

Appendix C (*continued*)

Fms	ID	Depth	TOC	S1	S2	HI	PP	PI	Tmax
	#	[m; MD]	[wt%]	[mg HC/g rock]		[mg HC/g TOC]	[mg HC/g rock]		[°C]
	12	2070.0	0.39	0.2	1.2	256	1.13	0.12	–
	13	2080.0	0.46	0.2	1.3	180	0.92	0.10	–
	14	2090.0	0.40	0.1	1.0	135	0.61	0.11	–
	15	2100.0	0.30	0.1	0.8	110	0.35	0.06	431
	16	2110.0	0.37	0.1	0.5	127	0.51	0.08	–
	17	2120.0	0.35	0.1	0.6	123	0.46	0.07	–
	18	2130.0	0.51	0.0	0.3	186	1.02	0.07	419
	19	2140.0	0.32	0.0	0.4	116	0.40	0.08	–
	20	2150.0	0.33	0.0	0.5	152	0.57	0.12	–
	21	2150.0	0.34	0.0	0.4	171	0.65	0.11	–
	22	2160.0	0.46	0.1	1.0	146	0.76	0.12	–
	23	2170.0	0.44	0.0	0.4	145	0.70	0.09	–
	24	2180.0	0.36	0.1	0.5	94	0.36	0.06	432
	25	2190.0	0.34	0.1	0.6	124	0.45	0.07	425
	26	2200.0	0.32	0.1	0.7	100	0.33	0.03	431
	27	2210.0	0.37	0.1	0.6	130	0.51	0.06	431
	28	2220.0	0.38	0.1	0.6	63	0.24	0.00	435
	29	2230.0	0.36	0.0	0.3	92	0.33	0.00	433
Tard Clay Formation	30	2235.0	1.35	0.0	0.4	378	5.71	0.11	437
	31	2240.0	1.43	0.0	0.3	418	6.57	0.09	438
	32	2245.0	1.71	0.0	0.5	411	7.91	0.11	437
	33	2250.0	1.89	0.0	0.2	439	9.31	0.11	436
	34	2255.0	1.42	0.0	0.3	377	6.07	0.12	436
	35	2260.0	1.38	0.6	5.1	372	5.77	0.11	438
	36	2265.0	1.15	0.6	6.0	307	3.96	0.11	438
	37	2270.0	0.94	0.9	7.0	280	2.93	0.10	439
	38	2275.0	0.94	1.0	8.3	249	2.64	0.11	438
	39	2280.0	0.76	0.7	5.4	270	2.25	0.09	439
	40	2285.0	0.76	0.6	5.1	243	2.04	0.09	438
	41	2290.0	0.92	0.4	3.5	189	1.94	0.10	439
	42*	2294.6	1.48	0.4	3.4	232	3.84	0.10	439
	43*	2296.5	0.94	0.3	1.8	186	2.05	0.14	439
	44*	2296.8	0.89	0.6	1.7	193	2.28	0.25	440
	45*	2297.6	0.99	0.4	1.9	187	2.24	0.17	441
	46*	2298.1	0.79	0.4	1.5	189	1.90	0.21	439
	47	2300.0	0.81	0.3	2.6	314	2.81	0.10	438
Buda Marl Formation	48	2305.0	0.31	0.3	2.3	194	0.61	0.02	437
	49	2310.0	0.21	0.2	2.1	119	0.25	0.00	437
	50	2315.0	0.06	0.2	1.9	117	0.07	0.00	436
	51	2320.0	0.21	0.2	1.7	33	0.07	0.00	434
	52	2325.0	0.04	0.3	2.5	225	0.10	0.10	437
	53	2330.0	0.26	0.0	0.6	77	0.24	0.17	436
	54	2335.0	0.18	0.0	0.3	50	0.09	0.00	435
	55	2340.0	0.27	0.0	0.1	119	0.37	0.14	438
	56	2345.0	0.24	0.0	0.1	63	0.19	0.21	437
	57	2350.0	0.71	0.0	0.1	165	1.47	0.20	438
	58	2355.0	2.61	0.0	0.2	271	8.16	0.13	430
	59	2360.0	2.65	0.0	0.1	258	7.90	0.14	433
	60	2365.0	0.34	0.1	0.3	88	0.33	0.09	437
	61	2370.0	0.30	0.0	0.2	117	0.37	0.05	434

Fms – formations, TOC – total organic carbon content, S1 – free hydrocarbons, S2 – hydrocarbons generated during Rock-Eval pyrolysis, HI – hydrogen index, PP – petroleum potential, PI – production index, Tmax – temperature of maximum hydrocarbon generation, MD – measured depth, * – drill core sample.

Appendix D. Supplementary data

Supplementary data to this article can be found online at https://doi.org/10.1016/j.marpetgeo.2021.104955.

References

Aquino Neto, F.R., Trendel, J.M., Restlé, A., Connan, J., Albrecht, P., 1983. Occurrence and formation of tricyclic terpanes in sediments and petroleums. In: Bjorøy, M., Albrecht, P., Cornford, C., de Groot, K., Eglinton, G., Galimov, E., Leythaeuser, D., Pelet, R., Rullkötter, J., Speers, G. (Eds.), Advances in Organic Geochemistry 1981. Wiley, Chichester, pp. 659–667.

Badics, B., Vető, I., 2012. Source rocks and petroleum systems in the Hungarian part of the Pannonian Basin: the potential for shale gas and shale oil plays. Mar. Petrol. Geol. 31, 53–69. https://doi.org/10.1016/j.marpetgeo.2011.08.015.

Báldi, T., 1984. The terminal Eocene and Early Oligocene events in Hungary and the separation of an anoxic, cold Paratethys. Eclogae Geol. Helv. 77, 1–27.

Báldi, T., Báldi-Beke, M., 1985. The evolution of the Hungarian paleogene basins. Acta Geol. Hung. 28, 5–28.

Bauer, M., M Tóth, T., 2017. Characterization and DFN modelling of the fracture network in a Mesozoic karst reservoir: Gomba oilfield, Paleogene Basin, Central Hungary. J. Pet. Geol. 40, 319–334. https://doi.org/10.1111/jpg.12678.

Bauer, M., M Tóth, T., Raucsik, B., Garaguly, I., 2016. Petrology and paleokarst features of the Gomba hydrocarbon reservoir (central Hungary). Centr. Eur. Geol. 59, 28–59. https://doi.org/10.1556/24.59.2016.003.

Bechtel, A., Hámor-Vidó, M., Gratzer, R., Sachsenhofer, R.F., Püttmann, W., 2012. Facies evolution and stratigraphic correlation in the early Oligocene Tard Clay of Hungary as revealed by maceral, biomarker and stable isotope composition. Mar. Petrol. Geol. 35, 55–74 https://doi.10.1016/j.marpetgeo.2012.02.017.

Bechtel, A., Gratzer, R., Linzer, H.-G., Sachsenhofer, R.F., 2013. Influence of migration distance, maturity and facies on the stable isotopic composition of alkanes and on carbazole distributions in oils and source rocks of the Alpine Foreland Basin of Austria. Org. Geochem. 62, 74–85.

Behar, F., Beaumont, V., De, B., Penteado, H., 2001. Rock-eval 6 Technology: performances and developments. Oil Gas Sci. Technol. 56, 111–134 https://doi.10.2516/ogst:2001013.

Bingham, E.M., McClymont, E.L., Väliranta, M., Mauquoy, D., Roberts, Z., Chambers, F. M., Evershed, R.P., 2010. Conservative composition of *n*-alkane biomarkers in Sphagnum species: implications for palaeoclimate reconstruction in ombrotrophic peat bogs. Org. Geochem. 41, 214–220. https://doi:10.1016/j.orggeochem.2009.06.010.

Bjorøy, M., Hall, P.B., Hustad, E., Williams, J.A., 1992. Variation in stable carbon isotope ratios of individual hydrocarbons as a function of artificial maturity. Org. Geochem. 19, 89–105. https://doi:10.1016/0146-6380(92)90029-w.

Bjorøy, M., Hall, P.B., Moe, R.P., 1994. Stable carbon isotope variation of *n*-alkanes in Central Graben oils. Org. Geochem. 22, 355–381. https://doi:10.1016/0146-6380(94)90114-7.

Blair, N., Leu, A., Muñoz, E., Olsen, J., Kwong, E., Des Marais, D., 1985. Carbon isotopic fractionation in heterotrophic microbial metabolism. Appl. Environ. Microbiol. 50, 996–1001 https://doi.10.1128/aem.50.4.996-1001.1985.

Blumer, M., Mullin, M.M., Thomas, D.W., 1963. Pristane in zooplankton. Science 140, 974. https://doi.org/10.1126/science.140.3570.974.

Final report of the hydrocarbon exploration activities in the area of 103. Gödöllő vol. I–II. MOL Plc. In: Boncz, L. (Ed.), 2004. Szolnok. MGSH Geological Data Store, T, p. 21172.

Final report of the hydrocarbon exploration activities in the area of 138. Monor vol. I–II. MOL Plc. In: Boncz, L. (Ed.), 2013. Szolnok. MGSH Geological Data Store, T, p. 22781.

Bordenave, M.L., Espitalié, J., Leplat, P., Oudin, J.L., Vandenbroucke, M., 1993. Screening techniques for source rock evaluation. In: Bordenave, M.L. (Ed.), Applied Petroleum Geochemistry. Éditions Technip, Paris, pp. 217–278.

Bray, E.E., Evans, E.D., 1961. Distribution of n-paraffins as a clue to recognition of source beds. Geochem. Cosmochim. Acta 22, 2–15. https://doi.org/10.1016/0016-7037(61)90069-2.

Brukner-Wein, A., Hetényi, M., Vető, I., 1990. Organic geochemistry of an anoxic cycle: a case history from the Oligocene section, Hungary. Org. Geochem. 15, 123–130. https://doi.org/10.1016/0146-6380(90)90077-d.

Casagrande, D.J., 1987. Sulphur in peat and coal. In: Scott, A.C. (Ed.), Coal and Coal-Bearing Strata: Recent Advances, vol. 32. Geological Society, London, Special Publications, pp. 87–105. https://doi:10.1144/gsl.sp.1987.032.01.07.

Cheng, P., Xiao, X.M., Gai, H.F., Li, T.F., Zhang, Y.Z., Huang, B.J., Wilkins, R.W.T., 2015. Characteristics and origin of carbon isotopes of *n*-alkanes in crude oils from the western Pearl River Mouth Basin, South China sea. Mar. Petrol. Geol. 67, 217–229 https://doi.10.1016/j.marpetgeo.2015.05.028.

Clayton, C.J., 1991. Effect of maturity on carbon isotope ratios of oils and condensates. Org. Geochem. 17, 887–899 https://doi.10.1016/0146-6380(91)90030-n.

Cloern, J.E., Canuel, E.A., Harris, D., 2002. Stable carbon and nitrogen isotope composition of aquatic and terrestrial plants of the San Francisco Bay estuarine system. Limnol. Oceanogr. 47, 713–729 https://doi.10.4319/lo.2002.47.3.0713.

Connan, J., Cassou, A.M., 1980. Properties of gases and petroleum liquids derived from terrestrial kerogen at various maturation levels. Geochem. Cosmochim. Acta 44, 1–23. https://doi:10.1016/0016-7037(80)90173-8.

Coplen, T.B., 2011. Guidelines and recommended terms for expression of stable-isotope-ratio and gas-ratio measurement results. Rapid Commun. Mass Spectrom. 25, 2538–2560. https://doi.org/10.1002/rcm.5129.

Cranwell, P.A., 1977. Organic geochemistry of cam loch (sutherland) sediments. Chem. Geol. 20, 205–221. https://doi.org/10.1016/0009-2541(77)90044-4.

Cranwell, P.A., Eglinton, G., Robinson, N., 1987. Lipids of aquatic organisms as potential contributors to lacustrine sediments – II. Org. Geochem. 11, 513–527. https://doi.org/10.1016/0146-6380(87)90007-6.

Dehmer, J., 1995. Petrological and organic geochemical investigation of recent peats with known environments of deposition. Int. J. Coal Geol. 28, 111–138. https://doi:10.1016/0166-5162(95)00016-x.

Didyk, B.M., Simoneit, B.R.T., Brassell, S.C., Eglinton, G., 1978. Organic geochemical indicators of palaeoenvironmental conditions of sedimentation. Nature 272, 216–222. https://doi.org/10.1038/272216a0.

Diefendorf, A.F., Freeman, K.H., Wing, S.L., Graham, H.V., 2011. Production of n-alkyl lipids in living plants and implications for the geologic past. Geochem. Cosmochim. Acta 75, 7472–7485 https://doi.10.1016/j.gca.2011.09.028.

Diefendorf, A.F., Sberna, D.T., Taylor, D.W., 2015. Effect of thermal maturation on plant-derived terpenoids and leaf wax n-alkyl components. Org. Geochem. 89–90, 61–70 https://doi.10.1016/j.orggeochem.2015.10.006.

Dolton, G.L., 2006. Pannonian Basin Province, Central Europe (Province 4808)—petroleum geology, total petroleum systems, and petroleum resource assessment. U. S. Geological Survey Bulletin 2204–B. https://doi.org/10.3133/b2204b.

Eglinton, G., Hamilton, R.J., 1967. Leaf epicuticular waxes. Science 156, 1322–1335. https://doi:10.1126/science.156.3780.1322.

Ekweozor, C.M., Okogun, J.I., Ekong, D.E.U., Maxwell, J.R., 1979. Preliminary organic geochemical studies of samples from the Niger delta (Nigeria) I. Analyses of crude oils for triterpanes. Chem. Geol. 27, 11–28. https://doi:10.1016/0009-2541(79)90100-1.

Ekweozor, C., Strausz, O., 1983. Tricyclic terpanes in the Athabasca oil sands: their geochemistry. In: Bjorøy, M., Albrecht, P., Cornford, C., de Groot, K., Eglinton, G., Galimov, E., Leythaeuser, D., Pelet, R., Rullkötter, J., Speers, G. (Eds.), Advances in Organic Geochemistry 1981. Wiley, Chichester, pp. 746–766.

Ensminger, A., Joly, G., Albrecht, P., 1978. Rearranged steranes in sediments and crude oils. Tetrahedron Lett. 19, 1575–1578 https://doi.10.1016/s0040-4039(01)94608-8.

Espitalié, J., LaPorte, J.L., Madec, M., Marquis, F., Leplat, P., Paulet, J., Boutefeu, A., 1977. Méthode rapide de charactérisation des roches metres, de leur potential pétrolier et de leur degé d'évolution. Rev. Inst. Fr. Petrol 32, 23–42. https://doi.org/10.2516/ogst:1977002.

Ficken, K.J., Li, B., Swain, D.L., Eglinton, G., 2000. An *n*-alkane proxy for the sedimentary input of submerged/floating freshwater aquatic macrophytes. Org. Geochem. 31, 745–749. https://doi.org/10.1016/s0146-6380(00)00081-4.

Ficken, K.J., Street-Perrott, F.A., Perrott, R.A., Swain, D.L., Olago, D.O., Eglinton, G., 1998. Glacial/interglacial variations in carbon cycling revealed by molecular and isotope stratigraphy of Lake Nkunga, Mt. Kenya, East Africa. Org. Geochem. 29, 1701–1719 https://doi.10.1016/s0146-6380(98)00109-0.

Fodor, L., Magyari, Á., Fogarasi, A., Palotás, K., 1994. Tertiary tectonics and late Palaeogene sedimentation in the Buda Hills, Hungary. A new interpretation of the Buda line. Bull. - Houst. Geol. Soc. 124, 129–305.

Gidai, L., 1978. A kósdi eocén képződmények rétegtani viszonyai (Conditions stratigraphiques des formations éocènes de Kósd). Bull. - Houst. Geol. Soc. 108, 65–86.

Goossens, H., de Leeuw, J.W., Schenck, P.A., Brassell, S.C., 1984. Tocopherols as likely precursors of pristane in ancient sediments and crude oils. Nature 312, 440–442. https://doi.org/10.1038/312440a0.

Grantham, P.J., Wakefield, L.L., 1988. Variations in the sterane carbon number distributions of marine source rock derived crude oils through geological time. Org. Geochem. 12, 61–73. https://doi.org/10.1016/0146-6380(88)90115-5.

Grice, K., de Mesmay, R., Glucina, A., Wang, S., 2008. An improved and rapid 5Å molecular sieve method for gas chromatography isotope ratio mass spectrometry of *n*-alkanes (C_8–C_{30+}). Org. Geochem. 39, 284–288.

Haas, J., Kovács, S., 2012. Pelso composite unit. In: Haas, J. (Ed.), Geology of Hungary. Springer-Verlag, Berlin, pp. 21–81.

Hertelendi, A., Vető, I., 1991. The marine photosynthetic carbon isotope fractionation remained constant during the Early Oligocene. Palaeogeogr. Palaeoclimatol. Palaeoecol. 83, 333–339. https://doi.org/10.1016/0031-0182(91)90059-z.

Huang, W.Y., Meinshein, W.G., 1979. Sterols as ecological indicators. Geochem. Cosmochim. Acta 43, 739–745. https://doi.org/10.1016/0016-7037(79)90257-6.

Hughes, W.B., Holba, A.G., Dzou, L.I.P., 1995. The ratios of dibenzothiophene to phenanthrene and pristan to phytan as indicators of depositional environment and lithology of petroleum source rocks. Geochem. Cosmochim. Acta 59, 3581–3598. https://doi.org/10.1016/0016-7037(95)00225-o.

Jacob, J., Disnar, J.-R., Boussafir, M., Spadano Albuquerque, A.L., Sifeddine, A., Turcq, B., 2007. Contrasted distributions of triterpene derivatives in the sediments of Lake Caçó reflect paleoenvironmental changes during the last 20,000 yrs in NE Brazil. Org. Geochem. 38, 180–197. https://doi:10.1016/j.orggeochem.2006.10.007.

Kázmér, M., 1985. Microfacies pattern of the upper Eocene limestones at budapest, Hungary. Ann. Univ. Sci. Budapestinensis Rol. Eotvos Nomin. Sect. Geol. 25, 139–152.

Kercsmár, Zs, Budai, T., Csillag, G., Selmeczi, I., Sztanó, O., 2015. Surface Geology of Hungary. Explanatory Notes to the Geological Map of Hungary (1:500 000). Geological and Geophysical Institute of Hungary, Budapest.

Final report of the hydrocarbon exploration activities in the area of 27. SW Hungarian Palaeogene Basin vol. I–II. MOL Plc. In: Kiss, K. (Ed.), 1999. Szolnok. MGSH Geological Data Store, T., Budapest.

Kokai, J., 1994. Exploration history and future possibilities in Hungary. In: Popescu, B.M. (Ed.), Hydrocarbons of Eastern Central Europe, Habitat, Exploration and Production History. Springer-Verlag, Berlin, pp. 147–173. https://doi:10.1007/978-3-642-77205-4_5.

Körmös, S., Bechtel, A., Sachsenhofer, R.F., Radovics, B.G., Milota, K., Schubert, F., 2020. Petrographic and organic geochemical study of the Eocene Kosd Formation (northern Pannonian Basin): implications for paleoenvironment and hydrocarbon source potential. Int. J. Coal Geol. 103555. https://doi:10.1016/j.coal.2020.103555.

Kovács, S., Haas, J., 2010. Displaced south alpine and dinaridic elements in the mid-Hungarian zone. Cent. Eur. Geol. 53, 135–164. https://doi:10.1556/ceugeol.53.2010.2-3.3.

Kováč, M., Plašienka, D., Soták, J., Vojtko, R., Oszczypko, N., Less, Gy, Ćosović, V., Fügenschuh, B., Králiková, S., 2016. Paleogene palaeogeography and basin evolution of the Western Carpathians, Northern Pannonian domain and adjoining areas. Global Planet. Change 140, 9–27. https://doi.org/10.1016/j.gloplacha.2016.03.007.

Lafargue, E., Marquis, F., Pillot, D., 1998. Rock-Eval 6 applications in hydrocarbon exploration, production, and soil contamination studies. Rev. Inst. Fr. Petrol 53, 421–437. https://doi.org/10.2516/ogst:1998036.

Lamb, A.L., Wilson, G.P., Leng, M.J., 2006. A review of coastal palaeoclimate and relative sea-level reconstructions using $\delta^{13}C$ and C/N ratios in organic material. Earth Sci. Rev. 75, 29–57. https://doi.org/10.1016/j.earscirev.2005.10.003.

Less, Gy, 2005. Palaeogene. In: Pelikán, P. (Ed.), Geology of the Bükk Mountains, Explanatory Book of the Geological Map of the Bükk Mountains (1:50 000). Hungarian Geological Society, Budapest, p. 204–210.

Lockheart, M.J., Van Bergen, P.F., Evershed, R.P., 1997. Variations in the stable carbon isotope compositions of individual lipids from the leaves of modern angiosperms: implications for the study of higher land plant-derived sedimentary organic matter. Org. Geochem. 26, 137–153 https://doi.10.1016/s0146-6380(96)00135-0.

Mackenzie, A.S., 1984. Application of biological markers in petroleum geochemistry. In: Brooks, J., Welte, D.H. (Eds.), Advances in Petroleum Geochemistry. Academic Press, London, pp. 115–214. https://doi.org/10.1016/b978-0-12-032001-1.50008-0.

Mackenzie, A.S., Brassell, S.C., Eglinton, G., Maxwell, J.R., 1982. Chemical fossils: the geological fate of steroids. Science 217, 491–504. https://doi.org/10.1126/science.217.4559.491.

Mackenzie, A.S., Maxwell, J.R., 1981. Assessment of thermal maturation in sedimentary rocks by molecular measurements. In: Brooks, J. (Ed.), Organic Maturation Studies and Fossil Fuel Exploration. Academic Press, London, pp. 239–254.
Maclean, L.C.W., Tyliszczak, T., Gilbert, P.U.P.A., Zhou, D., Pray, T.J., Onstott, C., Southam, G., 2008. A high-resolution chemical and structural study of framboidal pyrite formed within a low-temperature bacterial biofilm. Geobiology 6, 471–480. https://doi.org/10.1111/j.1472-4669.2008.00174.x.
Mayer, J., Sachsenhofer, R.F., Ungureanu, C., Bechtel, A., Gratzer, R., Sweda, M., Tari, G., 2018. Petroleum charge and migration in the Black Sea: insights from oil and source rock geochemistry. J. Petrol. Geol. 41, 337–350 https://doi.10.1111/jpg.12706.
Meyers, P.A., 1997. Organic geochemical proxies of paleoceanographic, paleolimnologic, and paleoclimatic processes. Org. Geochem. 27, 213–250. https://doi:10.1016/s0146-6380(97)00049-1.
Milota, K., Kovács, A., Galicz, Zs, 1995. Petroleum potential of the north Hungarian Oligocene sediments. Petrol. Geosci. 1, 81–87. https://doi.org/10.1144/petgeo.1.1.81.
Moldowan, J.M., Fago, F.J., Lee, C.J., Jacobson, S.R., Watt, D.S., Slougui, N.E., Jeganathan, A., Young, D.C., 1990. Sedimentary 24-n-propylcholestanes, molecular fossils diagnostic of marine algae. Science 247, 309–312. https://doi:10.1126/science.247.4940.309.
Morad, S., 1998. Carbonate cementation in sandstones: distribution patterns and geochemical evolution. Special Publ. Int. Assoc. Sedimentol. 26, 1–26. https://doi.org/10.1002/9781444304893.ch1.
Mortillaro, J.M., Passarelli, C., Abril, G., Hubas, C., Alberic, P., Artigas, L.F., Benedetti, M.F., Thiney, N., Moreira-Turcq, P., Perez, M.A.P., Vidal, L.O., Meziane, T., 2016. The fate of C4 and C3 macrophyte carbon in central Amazon floodplain waters: insights from a batch experiment. Limnol 59, 90–98 https://doi.10.1016/j.limno.2016.03.008.
Nagymarosy, A., 1983. Mono- and duospecific nannofloras in Early Oligocene sediments of Hungary. Palaeontology Proceedings B86, 273–283.
Nagymarosy, A., 2013. Hungarian Palaeogene Basin. In: Haas, J. (Ed.), Geology of Hungary. Springer, p. 83–102. https://doi:10.1007/978-3-642-21910-8.
Nagymarosy, A., Báldi-Beke, M., 1988. The position of the Paleogene Formations of Hungary in the standard Nannoplankton zonation. Ann. Univ. Sci. Budapestinensis Rol. Eotvos Nomin. Sect. Geol. 28, 3–25.
Nagymarosy, A., Báldi, T., Horváth, M., 1986. The Eocene/Oligocene boundary in Hungary. Dev. Palaentol. Stratigr. 113–116. https://doi:10.1016/s0920-5446(08)70103-1.
Nott, C.J., Xie, S., Avsejs, L.A., Maddy, D., Chambers, F.M., Evershed, R.P., 2000. *n*-Alkane distributions in ombrotrophic mires as indicators of vegetation change related to climate variation. Org. Geochem. 31, 231–235. https://doi.org/10.1016/s0146-6380(99)00153-9.
Ourisson, G., Albrecht, P., Rohmer, M., 1979. The hopanoids. Pure Appl. Chem. 51, 709–729.
Ozsvárt, P., Kocsis, L., Nyerges, A., Győri, O., Pálfy, J., 2016. The eocene-oligocene climate transition in the central Paratethys. Palaeogeogr. Palaeoclimatol. Palaeoecol. 459, 471–487. https://doi:10.1016/j.palaeo.2016.07.034.
Palotai, M., 2013. Oligocene–Miocene Tectonic Evolution of the Central Part of the Mid-Hungarian Shear Zone. Doctoral dissertation, Eötvös Loránd University, Budapest.
Pearson, E.J., Farrimond, P., Juggins, S., 2007. Lipid geochemistry of lake sediments from semi-arid Spain: relationships with source inputs and environmental factors. Org. Geochem. 38, 1169–1195 https://doi.10.1016/j.orggeochem.2007.02.007.
Pedentchouk, N., Turich, C., 2017. Carbon and hydrogen isotopic compositions of *n*-alkanes as a tool in petroleum exploration. In: Lawson, M., Formolo, M.J., EILER, J. M. (Eds.), From Source to Seep: Geochemical Applications in Hydrocarbon Systems, vol. 468. Geological Society, London, Special Publications, pp. 105–125. https://doi.org/10.1144/SP468.1.
Peters, K.E., 1986. Guidelines for evaluating petroleum source rocks using programmed pyrolysis. AAPG Bull. 70, 318–329. https://doi.org/10.1306/94885688-1704-11d7-8645000102c1865d.
Peters, K.E., Cassa, M.R., 1994. Applied source rock geochemistry. In: Magoon, L.B., Dow, G.W. (Eds.), The Petroleum System – from Source to Trap, vol. 60. AAPG Mem., Tulsa, Oklahoma, pp. 93–120.
Peters, K.E., Moldowan, J.M., 1991. Effects of source, thermal maturity, and biodegradation on the distribution and isomerization of homohopanes in petroleum. Org. Geochem. 17, 47–61. https://doi:10.1016/0146-6380(91)90039-m.
Peters, K.E., Moldowan, J.M., 1993. Interpreting Molecular Fossils in Petroleum and Ancient Sediments. The Biomarker Guide. Prentice Hall, Englewood Cliffs, N.J.
Peters, K.E., Moldowan, J.M., Driscole, A.R., Demaison, G.J., 1989. Origin of beatrice oil by co-sourcing from devonian and middle jurassic source rocks, inner moray firth, United Kingdom. AAPG Bull. 73, 454–471. https://doi.org/10.1306/c9ebcd51-1735-11d7-8645000102c1865d.
Peters, K.E., Snedden, J.W., Sulaeman, A., Sarg, J.F., Enrico, R.J., 2000. A new geochemical-sequence stratigraphic model for the mahakam delta and makassar slope, kalimantan, Indonesia. AAPG Bull. 84, 12–44. https://doi.org/10.1306/e4fd386f-1732-11d7-8645000102c1865d.
Peters, K.E., Walters, C.C., Moldowan, J.M., 2005. The Biomarker Guide, second ed. Cambridge University Press, Cambridge.
Popov, S.V., Akhmetiev, M.A., Bugrova, E.M., Lopatin, A.V., Amitrov, O.V., Andreeva-Grigorovich, A.S., Zherikhin, V.V., Zaporozhets, N.I., Nikolaeva, I.A., Krasheninnikov, V.A., Kuzmicheva, E.I., Sytchevskaya, E.K., Shcherba, I.G., 2001. Biogeography of the northern peri-tethys from the late Eocene to the early Miocene: Part 1. Late Eocene. Paleontol. J. 35.
Popov, S.V., Rögl, F., Rozanov, A.Y., Steininger, F.F., Shcherba, I.G., Kovac, M., 2004. Lithological-Palaeogeographic Maps of Paratethys: 10 Maps Late Eocene to Pliocene. Courier Forschungsinstitut Senckenberg, Frankfurt.
Radke, M., Schaefer, R.G., Leythaeuser, D., Teichmüller, M., 1980a. Composition of soluble organic matter in coals: relation to rank and liptinite fluorescence. Geochem. Cosmochim. Acta 44, 1787–1800. https://doi.org/10.1016/0016-7037(80)90228-8.
Radke, M., Welte, D.H., 1983. The Methylphenanthrene Index (MPI): a maturity parameter based on aromatic hydrocarbons. In: Bjorøy, M. (Ed.), Advances in Org. Geochem. Wiley, Chichester, pp. 504–512.
Radke, M., Welte, D.H., Willsch, H., 1982a. Geochemical study of a well in the Western Canada Basin: relation of aromatic distribution pattern to maturity of organic matter. Geochem. Cosmochim. Acta 46, 1–10. https://doi.org/10.1016/0016-7037(82)90285-x.
Radke, M., Willsch, H., Leythaeuser, D., 1982b. Aromatic components of coal: relation of distribution pattern to rank. Geochem. Cosmochim. Acta 46, 1831–1848. https://doi.org/10.1016/0016-7037(82)90122-3.
Radke, M., Willsch, H., Welte, D.H., 1980b. Preparative hydrocarbon group type determination by automated medium pressure liquid chromatography. Anal. Chem. 52, 406–411. https://doi.org/10.1021/ac50053a009.
Rohmer, M., 1993. The biosynthesis of triterpenoids of the hopane series in the Eubacteria: a mine of new enzymatic reactions. Pure Appl. Chem. 65, 1293–1298. https://doi:10.1351/pac199365061293.
Rooney, M.A., Vuletich, A.K., Griffith, C.E., 1998. Compound-specific isotope analysis as a tool for characterizing mixed oils: an example from the West of Shetlands area. Org. Geochem. 29, 241–254. https://doi:10.1016/s0146-6380(98)00136-3.
Rowland, S.J., 1990. Production of acyclic isoprenoid hydrocarbons by laboratory maturation of methanogenic bacteria. Org. Geochem. 15, 9–16. https://doi.org/10.1016/0146-6380(90)90181-X.
Rögl, F., 1999. Mediterranean and Paratethys. Facts and hypotheses of an Oligocene to Miocene paleogeography (short overview). Geol. Carpathica 50, 339–349.
Sachsenhofer, R.F., Popov, S.V., Bechtel, A., Coric, S., Francu, J., Gratzer, R., Grunert, P., Kotarba, M., Mayer, J., Pupp, M., Rupprecht, B.J., 2018a. Oligocene and lower Miocene source rocks in the Paratethys: palaeogeographic and stratigraphic controls. In: Simmons, M. (Ed.), Petroleum Geology of the Black Sea, vol. 464. Geol. Soc. Spec. Publ, pp. 267–306. https://doi.org/10.1144/SP464.1.
Sachsenhofer, R.F., Popov, S.V., Coric, S., Mayer, J., Misch, D., Morton, M.T., Pupp, M., Rauball, J., Tari, G., 2018b. Paratethyan petroleum source rocks: an overview. J. Petrol. Geol. 41, 219–245. https://doi:10.1111/jpg.12702.
Sachsenhofer, R.F., Gratzer, R., Bechtel, A., 2019. Application of compound-specific carbon isotope analysis to improved oil-source correlations in the Paratethys area. In: Tari, G., Sachsenhofer, R.F. (Eds.), Paratethys Petroleum Systems between Central Europe and the Caspian Region. AAPG, Wien, p. 14.
Schmid, S.M., Bernoulli, D., Fügenschuh, B., Matenco, L., Schefer, S., Schuster, R., Tischler, M., Ustaszewski, K., 2008. The Alpine-Carpathian-Dinaridic orogenic system: correlation and evolution of tectonic units. Swiss J. Geosci. 101, 139–183. https://doi:10.1007/s00015-008-1247-3.
Schoell, M., 1984. Stable isotopes in petroleum research. Adv. Petrol. Geochem. 215–245. https://doi:10.1016/b978-0-12-032001-1.50009-2.
Schulz, H.-M., Bechtel, A., Sachsenhofer, R.F., 2005. The birth of the Paratethys during the early Oligocene: from tethys to an ancient Black Sea analogue? Global Planet. Change 49, 163–176. https://doi:10.1016/j.gloplacha.2005.07.001.
Schulz, H.-M., Sachsenhofer, R.F., Bechtel, A., Polesny, H., Wagner, L., 2002. The origin of hydrocarbon source rocks in the Austrian Molasse Basin (Eocene–Oligocene transition). Mar. Petrol. Geol. 19, 683–709. https://doi:10.1016/s0264-8172(02)00054-5.
Seifert, W.K., Moldowan, J.M., 1978. Applications of steranes, terpanes and monoaromatics to the maturation, migration and source of crude oils. Geochem. Cosmochim. Acta 42, 77–95. https://doi:10.1016/0016-7037(78)90219-3.
Seifert, W.K., Moldowan, J.M., 1980. The effect of thermal stress on source-rock quality as measured by hopane stereochemistry. Phys. Chem. Earth 12, 229–237. https://doi.org/10.1016/0079-1946(79)90107-1.
Seifert, W.K., Moldowan, J.M., 1986. Use of biological markers in petroleum exploration. In: Johns, R.B. (Ed.), Methods in Geochemistry and Geophysics 24. Elsevier, Amsterdam, pp. 261–290.
Shah, S.R., Griffith, D.R., Galy, V., McNichol, A.P., Eglinton, T.I., 2013. Prominent bacterial heterotrophy and sources of ^{13}C-depleted fatty acids to the interior Canada Basin. Biogeosciences 10, 7065–7080 https://doi.10.5194/bg-10-7065-2013.
Sieskind, O., Joly, G., Albrecht, P., 1979. Simulation of the geochemical transformation of sterols: superacid effect of clay minerals. Geochem. Cosmochim. Acta 43, 1675–1680. https://doi.org/10.1016/0016-7037(79)90186-8.
Sofer, Z., 1984. Stable carbon isotope compositions of crude oils: application to source depositional environments and petroleum alteration. AAPG Bull. 68, 31–49. https://doi:10.1306/ad460963-16f7-11d7-8645000102c1865d.
Summons, R.E., Volkman, J.K., Boreham, C.J., 1987. Dinosterane and other steroidal hydrocarbons of dinoflagellate origin in sediments and petroleum. Geochem. Cosmochim. Acta 51, 3075–3082 https://doi.10.1016/0016-7037(87)90381-4.
Sweeney, R.E., Kaplan, I.R., 1973. Pyrite framboid formation: laboratory synthesis and marine sediments. Econ. Geol. 68, 618–634. https://doi.org/10.2113/gsecongeo.68.5.618.
Sztanó, O., Tari, G., 1993. Early Miocene basin evolution in Northern Hungary: tectonics and eustasy. Tectonophysics 261, 485–502. https://doi.org/10.1016/0040-1951(93)90134-6.
Tao, S., Wang, C., Du, J., Liu, L., Chen, Z., 2015. Geochemical application of tricyclic and tetracyclic terpanes biomarkers in crude oils of NW China. Mar. Petrol. Geol. 67, 460–467. https://doi.org/10.1016/j.marpetgeo.2015.05.030.

Tari, G., Báldi, T., Báldi-Beke, M., 1993. Paleogene retroarc flexural basin beneath the Neogene Pannonian Basin: a geodynamic model. Tectonophysics 226, 433–455. https://doi:10.1016/0040-1951(93)90131-3.

Teece, M.A., Fogel, M.L., Dollhopf, M.E., Nealson, K.H., 1999. Isotopic fractionation associated with biosynthesis of fatty acids by a marine bacterium under oxic and anoxic conditions. Org. Geochem. 30, 1571–1579 https://doi.10.1016/s0146-6380(99)00108-4.

ten Haven, H.L., de Leeuw, J.W., Peakman, T.M., Maxwell, J.R., 1986. Anomalies in steroid and hopanoid maturity indices. Geochem. Cosmochim. Acta 50, 853–855. https://doi:10.1016/0016-7037(86)90361-3.

ten Haven, H.L., de Leeuw, J.W., Rullkötter, J., Sinninghe Damsté, J.S., 1987. Restricted utility of the pristane/phytane ratio as a palaeoenvironmental indicator. Nature 330, 641–643. https://doi.org/10.1038/330641a0.

Tissot, B.T., Welte, D.H., 1984. Petroleum Formation and Occurrences. Springer, Berlin.

Volkman, J.K., Allen, D.I., Stevenson, P.L., Burton, H.R., 1986. Bacterial and algal hydrocarbons from a saline Antarctic lake, Ace Lake. Org. Geochem. 10, 671–681. https://doi.org/10.1016/s0146-6380(86)80003-1.

Volkman, J.K., Barrett, S.M., Blackburn, S.I., 1999. Eustigmatophyte microalgae are potential sources of C_{29} sterols, C_{22}–C_{28} *n*-alcohols and C_{28}–C_{32} *n*-alkyl diols in freshwater environments. Org. Geochem. 30, 307–318. https://doi.org/10.1016/S0146-6380(99)00009-1.

Volkman, J.K., Maxwell, J.R., 1986. Acyclic isoprenoids as biological markers. In: Johns, R.B. (Ed.), Biological Markers in the Sedimentary Record. Elsevier, New York, pp. 1–42.

Wakeham, S.G., Amann, R., Freeman, K.H., Hopmans, E.C., Jørgensen, B.B., Putnam, I.F., Schouten, S., Sinninghe Damsté, J.S., Talbot, H.M., Woebken, D., 2007. Microbial ecology of the stratified water column of the Black Sea as revealed by a comprehensive biomarker study. Org. Geochem. 38, 2070–2097 https://doi.10.1016/j.orggeochem.2007.08.003.

Wingert, W.S., Pomerantz, M., 1986. Structure and significance of some twenty-one and twenty-two carbon petroleum steranes. Geochem. Cosmochim. Acta 50, 2763–2769. https://doi:10.1016/0016-7037(86)90225-5.

Wolff, G.A., Lamb, N.A., Maxwell, J.R., 1986. The origin and fate of 4-methyl steroid hydrocarbons. I. Diagenesis of 4-methyl sterenes. Geochem. Cosmochim. Acta 50, 335–342. https://doi:10.1016/0016-7037(86)90187-0.

Woodhouse, A.D., Oung, J.-N., Philp, R.P., Weston, R.J., 1992. Triterpanes and ring-A degraded triterpanes as biomarkers characteristic of Tertiary oils derived from predominantly higher plant sources. Org. Geochem. 18, 23–31. https://doi:10.1016/0146-6380(92)90140-s.

Xiao, H., Li, M., Liu, J., Mao, F., Cheng, D., Yang, Z., 2019. Oil-oil and oil-source rock correlations in the Muglad Basin, Sudan and South Sudan: new insights from molecular markers analyses. Mar. Petrol. Geol. 103, 351–365. https://doi:10.1016/j.marpetgeo.2019.03.004.

Xiao, H., Wang, T.-G., Li, M., Fu, J., Tang, Y., Shi, S., Yang, Z., Lu, X., 2018. Occurrence and distribution of unusual tri- and tetracyclic terpanes and their geochemical significance in some Paleogene oils from China. Energy Fuels 32, 7393–7403. https://doi.org/10.1021/acs.energyfuels.8b01025.